CHAPTER 3

PETROPHYSICAL INTERPRETATION

The wireline logging provides valuable information to evaluate the characteristics of potential reservoir. The descriptive features of well-logs could be traced to depositional environments. Since the reservoir properties such as porosity, permeability, effective thickness and major detrital composition; shale, sandstone and conglomerates restrained to the pattern of log response under associated depositional environments and diagenetic process.

3.1 Data verification

Gamma ray (GR), laterolog shallow (LLS), laterolog deep (LLD), microspherical focus log (MSFL), sonic, density, neutron and caliper logs are applied successively in this study.

The logging tools are recoding under slim hole conditions therefore they are unable to encounter the real conditions of environments. For accurate measurement of well-logs, a correction is applied to compensate for their borehole environments. Procedures of correction for available logs parameters are as follows.

- Correcting resistivity with shoulder bed, invasion, bed thickness and dip correction.
- Correcting density and neutron logs with caliper log.
- Borehole size, temperature and pressure are used for correcting neutron log.

Spontaneous potential (Sp) logs are absent in all wells so the baseline shift could not be done. All log curves were matched with their represented depths. Since there are no relevant processing data such as Drho (Δρ), Hdra, and, mud properties (weight, salinity, resistivity of mud, mud cake and mud filtration, and composition), the correction is not carried out in this study.

The surface positions of these wells are set at 2.5 m above sea level. Wells are drilled in deviated plan to target horizons except for well B. The measurement depths (MD) were therefore recalculated to true vertical depth (TVD) and true vertical depth subsea (TVDss).

3.2 Well correlation

Interpretation of stratigraphic horizon and relative structure features can be approached by using well-logs correlation. Gamma ray, sonic and resistivity logs are applied to correlate specific stratigraphic sections from one well to another. The significant characteristics of well-log pattern especially gamma ray and sonic logs were used to determine stratigraphic markers (horizons).

The significant features of gamma ray crossing over with sonic logs under relative scale could be classified as shale-break layer and non-shale body. High and sharp peak characters of gamma ray logs were determined as flooding surface horizon (top of unit KR1-1, KR2-1 and KR2-8A). The typical top of units were observed and traced on shale breaks. The bases of units were recognized alternately to the top of underlying units. The correlation was emphasized only for stratigraphic continuity. It was based on broad scale correlation by well positioning, and therefore, the structure

features between wells were not identified. Figure 3.1 illustrates the relative position of wells on surface and subsurface.

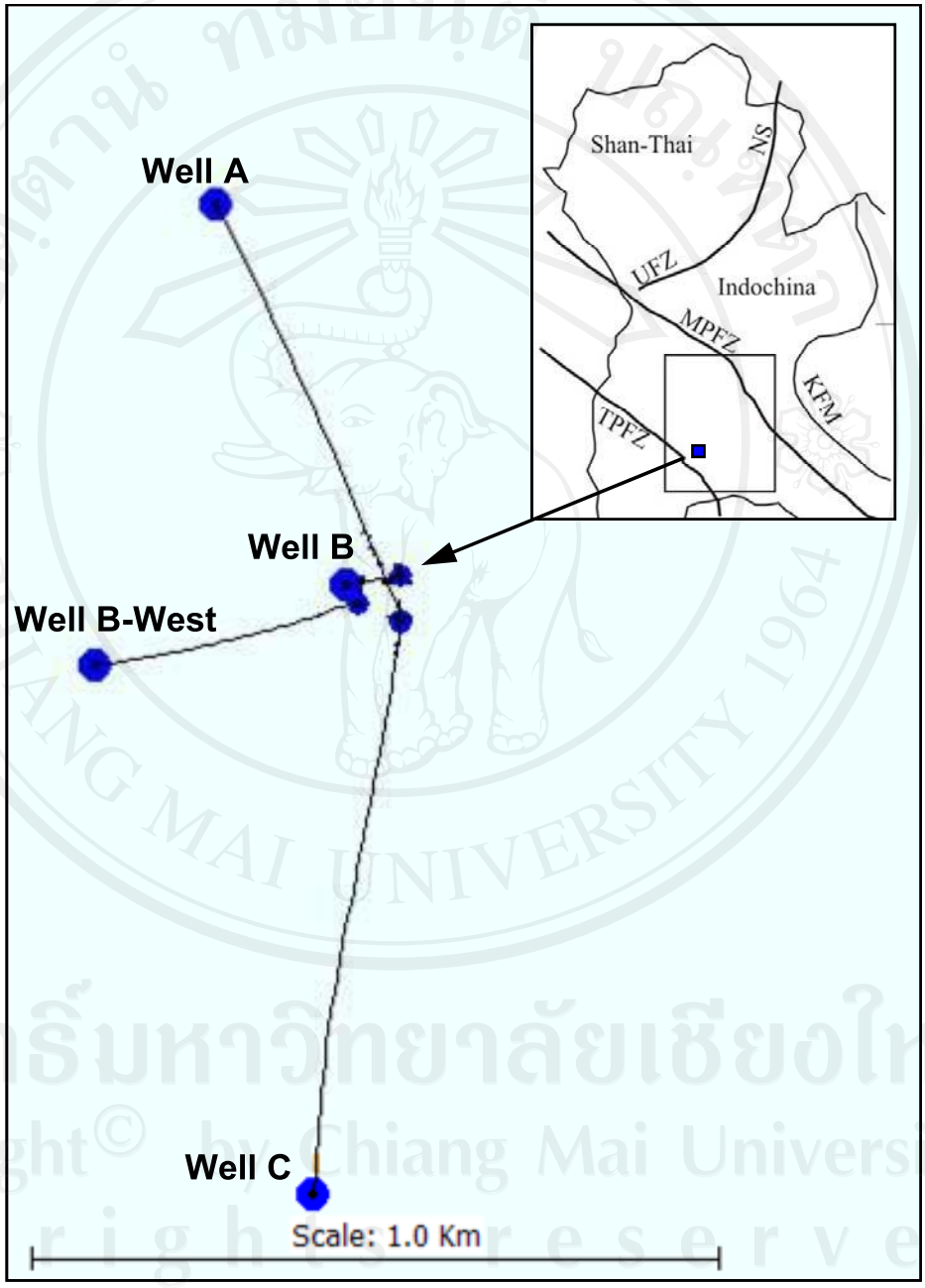

Figure 3.1 Relative layout plan of well-locations with their surface and subsurface positions (well names with large blue circles are subsurface positions).

The nomenclatures of correlated units were referenced from PTTEP (Tongpenyai et al., 2000). In 1993, PTTEP classified and revised the detail of the potential reservoirs into five units, namely A, B, C, D, and E units. Main oil reservoir, unit D, is subdivided to seven sub-units as D1 to D7. Among these seven sub-units, D2, D3, and D4 trapped main hydrocarbon of U-Thong oil field. Sub-units of D2 consist of reservoir units KR1-1, KR1-2, and KR1-3. The complete section of D3 was subdivided into reservoir units KR2-1, KR2-2, KR2-3, KR2-4, KR2-5, KR2-6, and KR2-7. KR2-8 was defined in D4. These reservoir units are middle to upper Miocene in age.

The logs were stacked and have been correlated under true vertical depth subsea (TVDss) and flatten to sea level (Figure 3.2). The reservoir zonings are comparatively deeper southward and shallow to north-east. The KR1-1 was considered as the top of first persistent reservoir unit beneath flooded shale. The flooded surface could be determined with a clear peak (high) gamma ray crossing over with sonic logs.

The positions of wells in Figure 3.2 were arranged into a north-south section. Well B-West is therefore in-line in an east-west direction with well B.

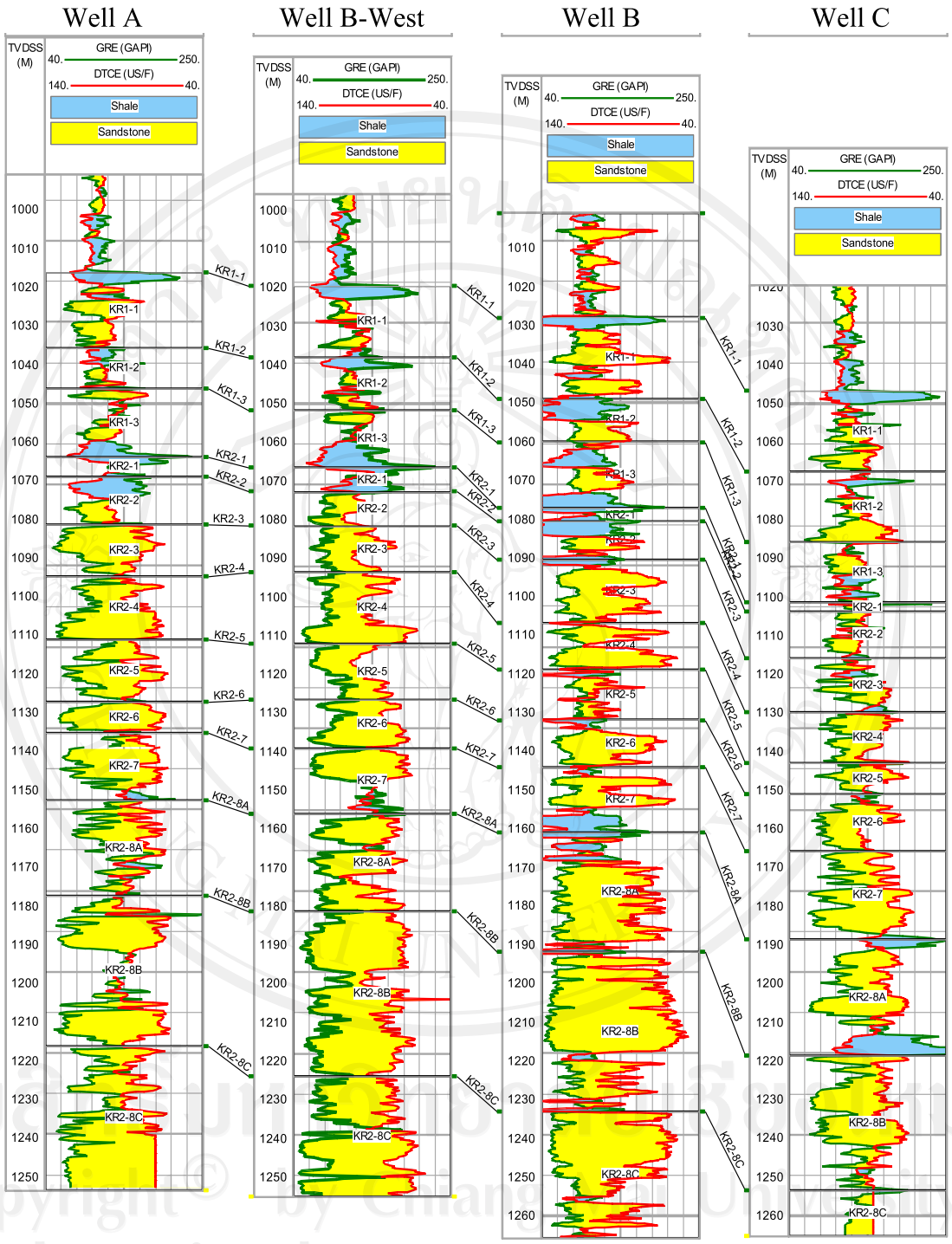

Figure 3.2 Correlation of wells using gamma ray and sonic logs (depth with TVDss and datum to sea level).

The Figure 3.2 shows the increase in the ratio of sand/shale with depth. The correlations with depth of reservoir units were listed in Table 3.1.

Table 3.1 Representative elevation of the tops of reservoir units with measured depth (MD) and true vertical depth subsea (TVDss) in meter.

Reservoir Units		A		B-West		B		C	
		Top	Btm.	Top	Btm.	Top	Btm.	Top	Btm.
KR1-1	MD	1173	1199	1071	1092	1037	1059	1293	1324
	TVDss	1016	1036	1020	1038	1028	1049	1047	1068
KR1-2	MD	1199	1212	1092	1106	1059	1071	1324	1351
	TVDss	1036	1046	1038	1052	1049	1062	1068	1086
KR1-3	MD	1212	1235	1106	1123	1071	1086	1051	1373
	TVDss	1046	1064	1052	1067	1062	1077	1086	1102
KR2-1	MD	1235	1242	1223	1230	1086	1090	1373	1376
	TVDss	1164	1169	1067	1073	1077	1081	1102	1104
KR2-2	MD	1235	1242	1123	1130	1090	1100	1373	1376
	TVDss	1069	1081	1073	1082	1081	1091	1104	1116
KR2-3	MD	1258	1276	1139	1153	1100	1116	1393	1413
	TVDss	1181	1195	1082	1094	1091	1107	1116	1130
KR2-4	MD	1276	1297	1153	1173	1116	1128	1413	1431
	TVDss	1095	1111	1094	1112	1107	1119	1130	1143
KR2-5	MD	1297	1318	1173	1189	1128	1141	1431	1442
	TVDss	1111	1127	1112	1127	1119	1132	1143	1151
KR2-6	MD	1378	1329	1189	1203	1141	1153	1442	1463
	TVDss	1127	1135	1127	1139	1132	1144	1151	1166
KR2-7	MD	1329	1351	1203	1222	1153	1170	1463	1495
	TVDss	1135	1153	1139	1156	1144	1161	1166	1189
KR2-8A	MD	1351	383	1222	1250	1170	1201	1495	1534
	TVDss	1153	1178	1156	1181	1161	1192	1189	1217
KR2-8B	MD	1383	1433	1250	1297	1201	1242	1534	1584
	TVDss	1178	1217	1181	1224	1192	1233	1217	1254
Total	MD	260		226		206		291	
	TVDss	201		205		205		207	

Btm. = Bottom

3.3 Well log interpretation

The interpretation was mainly objective to the interpretation of shaly sand models. Although there are many models accessible in shaly sand reservoir, only representative models with available log parameters were considered for interpretation. The shaly sand models were divided into three phase of calculation. They are estimating to volume of shale (Vsh), total and effective porosity (ϕ_t, ϕ_e) and water saturation (Sw) under relevant models.

An objective of this study is to asses as to which models are most applicable to establish reservoir characteristics in study area. Although the Archie model was designed for using in clean sand formation, it was applied to compare with other shaly sand models such as the Simandoux model, Modified Simandoux model, Poupon-Leveaus Indonesian model, and Dual Water model. The global parameters of well logs are set primarily as below.

Saturation component (n) = 2

Porosity factor or Tortuosity factor (a) = 1

Mean surface temperature = 26.7° C

Regional temperature gradient (G) = 4.7° C/100m

Type of rock matrix for density log = Sandstone

Density rock matrix (ρ_b) = 2.65 ~ 2.68 g/cc

Type of drilling fluid /density (ρ_f) = Salt water / 1.1 g/cc

Oil properties = 33 API° (density 0.8602)

Sonic transit time for sandstone matrix (Δt_{ma}) = 55.5 μs/ft (182 μs/m)

Sonic transit time for the pore filled with salt water (Δt_f)

= 185μs/ft (607 μs/m)

3.4 Volume of shale (Vsh) estimation

The volume of shale is an essential parameter for shaly sand analysis. There is no single or combination of petrophysical logs can accurately determine the shale content in all formations (Dewan, 1983). The shaly sand analyses were considered to prove the important scale of clay volumes in estimating effective porosity and effective water saturation. Gamma ray (Clavier method) and neutron-density clay indicators were used to differentiate the shale content and non-shale (matrix) content. The traditional procedures for concluding volume of shale resulted in the lowest values.

The estimating of Vsh using gamma ray method is the most popular and probably one of the accurate methods (Asquit, 1990, and Hilchie, 1982). According to traditional practice, using gamma ray to generate the volume of shale is minimized and more reliable than applying neutron-density in this study area. Figure 3.3 expressed the comparable result of Vsh estimated by using gamma ray and neutron-density logs. Well B-West adopted the volume of shale by gamma ray log only, since neutron-density logs are absent for this well. Comparative results of volume of shale were listed in Table 3.2. These results were objective to concern the contrasting Vsh laterally and vertically in each unit. The arithmetic method was applied to summarize the average of Vsh in Table 3.2.

Calculation of average volume of shale:

$$V_{sh.av} = \frac{\sum_{i=1}^{i=n} V_{sh.i} \times h_i}{\sum_{i=1}^{i=n} h_i}$$

where i= i^{th} input value
hi= i^{th} input interval
n= number of samples.

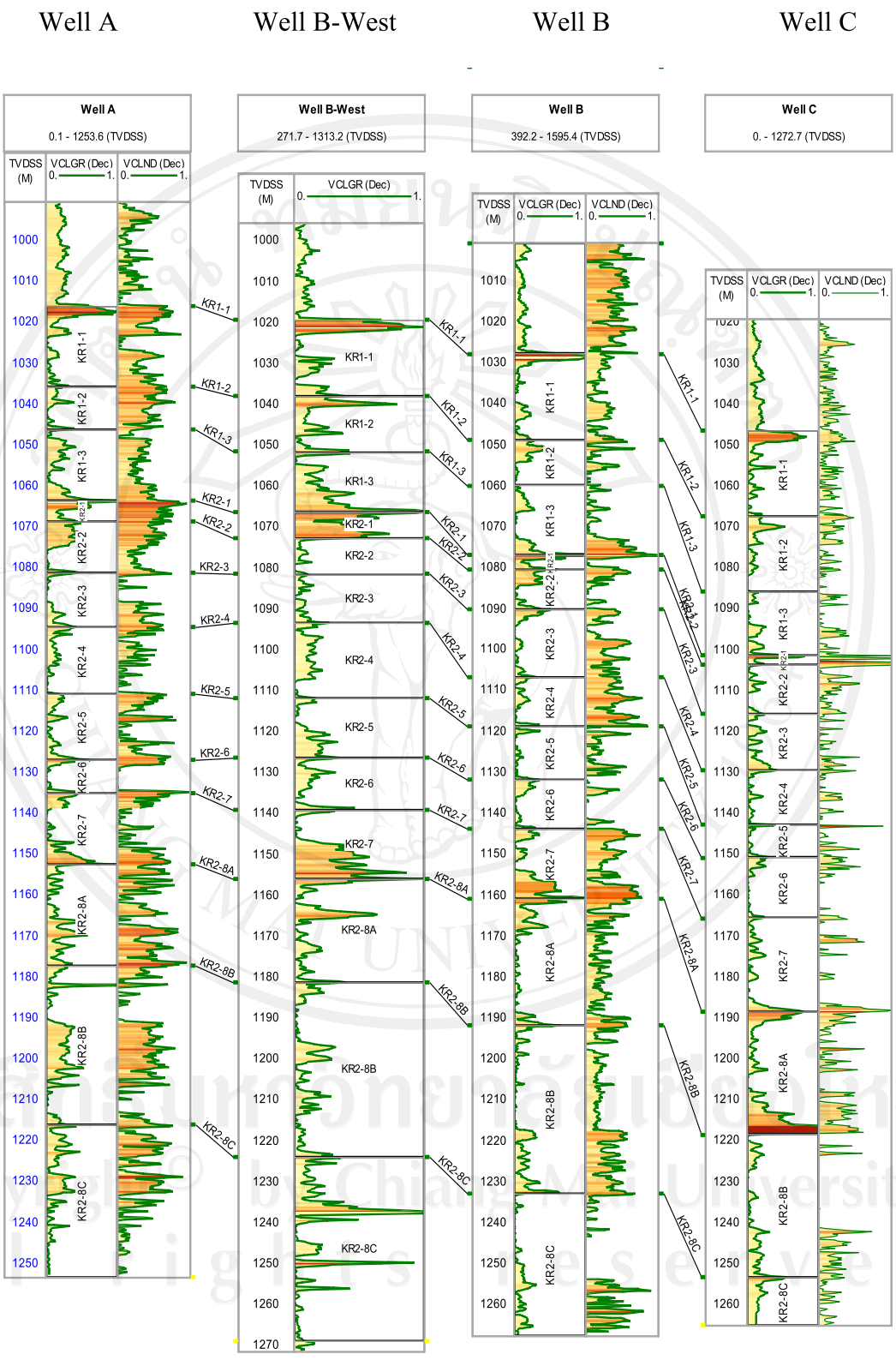

Figure 3.3. Volume of shale calculation based on gamma ray (Clavier method) and neutron-density method.

Table 3.2. Average Vsh comparison between gamma ray (clavier method) and neutron-density method.

WELL	A		B-West	B		C	
Reservoir Unit	Vsh.GR	Vsh.ND	Vsh.GR	Vsh.GR	Vsh.ND	Vsh.GR	Vsh.ND
KR1-1	14	39	17	10	23	18	17
KR1-2	12	50	18	15	21	14	18
KR1-3	20	33	25	15	24	14	20
KR2-1	39	71	50	31	22	18	41
KR2-2	22	41	8	24	25	8	23
KR2-3	14	34	8	10	30	20	18
KR2-4	14	27	11	11	46	10	18
KR2-5	15	37	13	5	22	9	22
KR2-6	16	33	13	13	20	16	23
KR2-7	21	35	26	23	41	16	28
KR2-8A	18	46	11	12	24	25	25
KR2-8B	23	40	9	10	27	17	25

where Vsh-GR= Volume of shale calculated using gamma ray

Vsh-ND= Volume of shale calculated using neutron-density.

The clavier formula of gamma ray method was preferred in estimation of Vsh for the study area. Based on the core samples, the reservoir units are clay supported lithic sandstone and conglomerate. Therefore, the method was more appropriate in estimating Vsh if compared with others formulae.

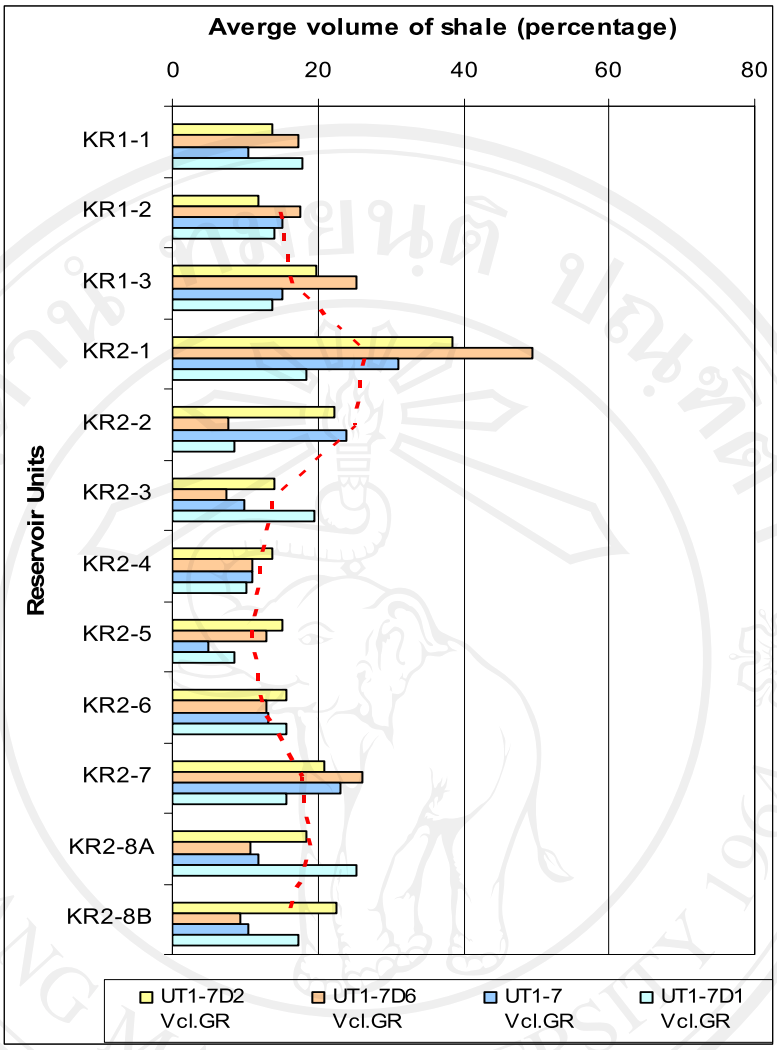

Figure 3.4 Average values of Vsh based on the gamma ray (clavier method).

According to the results of Vsh in Figure 3.4, the eastern part of the studying area (well B) comprises relatively low amount of average Vsh. The highest volume of average Vsh (50%) was recorded in unit KR2-1 of well B-West. Well B displays the 5% of minimum Vsh in unit KR2-5. In the northern and southern areas, well A and well C have 19% and 15% of average Vsh respectively. Increasing and decreasing amount of average Vsh with depth were traced with the red dotted line in Figure 3.4. That line could be recognized as the fluctuation level of local tide (distribution of depositional energy).

3.5 Effective porosity estimation of shaly sand formation (ϕ_e)

Effective porosity is the most important parameter to determine the properties of a reservoir. The quality of porosity in potential reservoir is directly related to the economic evaluations. The estimation is the key to concern the quantity of effective water saturation especially in shaly sand. “Clay surfaces and interlayer” comprised electrochemically bound water (clay bound water, CBW) which varies in volume according to the clay-type and the salinity of the formation water. The most common definition of effective porosity for clastic reservoirs excludes clay bound water, whereas it is composed as part of the total porosity (Worthington, 2005).

Eslinger and Pevear (1988) classified types of effective porosity in shaly sand formation (Figure 3.5). Figure 3.5 compares the porosities of under laboratory analysis and based on neutron-density values.

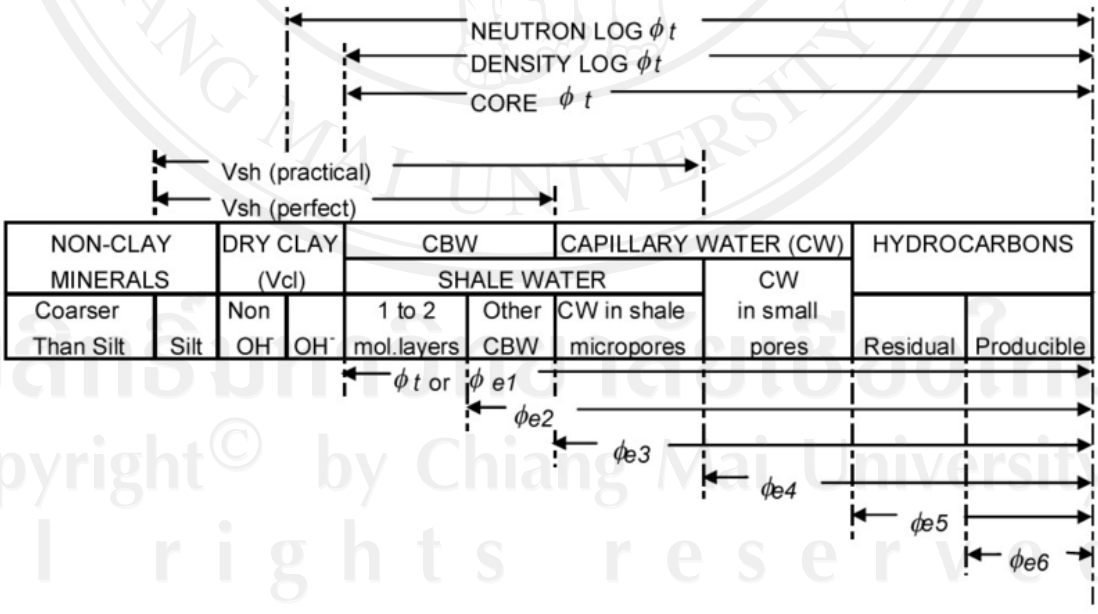

Figure 3.5. Classification of different types of effective porosity (by Eslinger and Pevear, 1988).

The following terms are represented to Figure 3.5 and described as follows.

ϕ_t = Total porosity, volume of the reservoir rock which is fluid (oil, water, and gas) filled.

ϕ_{e1} = Effective porosity, the sum of all the interconnected pore space. In the vast majority of cases, this core analysis and petroleum engineering definition of effective porosity equates to total porosity.

ϕ_{e2} = Effective porosity measured on core samples which are dried in a humidity oven so that clays retain one or two molecular layers of bound water however, this CBW tends to a minimum and is likely not reservoir representative.

ϕ_{e3} = Effective porosity, total porosity minus clay-bound water (CBW).

ϕ_{e4} = Effective porosity, log effective porosity. In essence, total porosity minus shale water, where solid minerals and the volume of shale (Vsh) constitute the matrix (non-effective porosity) and the remaining volume constitutes the effective porosity.

ϕ_{e5} = Effective porosity, in a hydrocarbon-bearing reservoir above the transition zone, only that pore space which is filled with hydrocarbons. From the nuclear magnetic resonance (NMR) log, this equates to the Free Fluid Index (FFI), in other words, all pore space above the T2 cut-off.

ϕ_{e6} = Effective porosity, that volume of pore space which contains only producible hydrocarbons.

Clay Bound Water (CBW) = Total porosity × SF × Qv

SF = Salinity Factor ($0.6425 * S^{-0.5} + 0.22$)

S= Salinity, g/l

Qv = Cation Exchange Capacity, meq/ml pore space

Neutron, density and sonic logs are commonly used to estimate porosity. The variations of neutron and density logs are usually used to estimate porosity and to focus on the presence of hydrocarbon. The different types of rock units and presence of hydrocarbon can be identified on the separation between the neutron and density logs. The larger separation of high neutron and low density readings are evidence of shale units while clean sand correspond to closed neutron and density responses. Alternately, the presence of hydrocarbon is indicated by the crossing over of neutron and density logs at appropriate scale.

In this field application, the contrast between neutron-density logs is obscure to predict the trace of hydrocarbon zone with the presence of shale. Neutron-density porosities are estimated for three wells except for the well B-West. The well B-West has only sonic log available for porosity computation.

Figure 3.6 compares porosities based on neutron, density (Dewan, 1983) and sonic logs (Wyllie, 1958). Table 3.3 lists the average of effective porosity calculated by Arithmetic method.

Average effective porosity by Arithmetic method: $$\phi_{e.av} = \frac{\sum_{i=1}^{i=n} \phi_i \times h_i}{\sum_{i=1}^{i=n} h_i}$$

where i= i^{th} input value

hi= i^{th} input interval

n= number of samples.

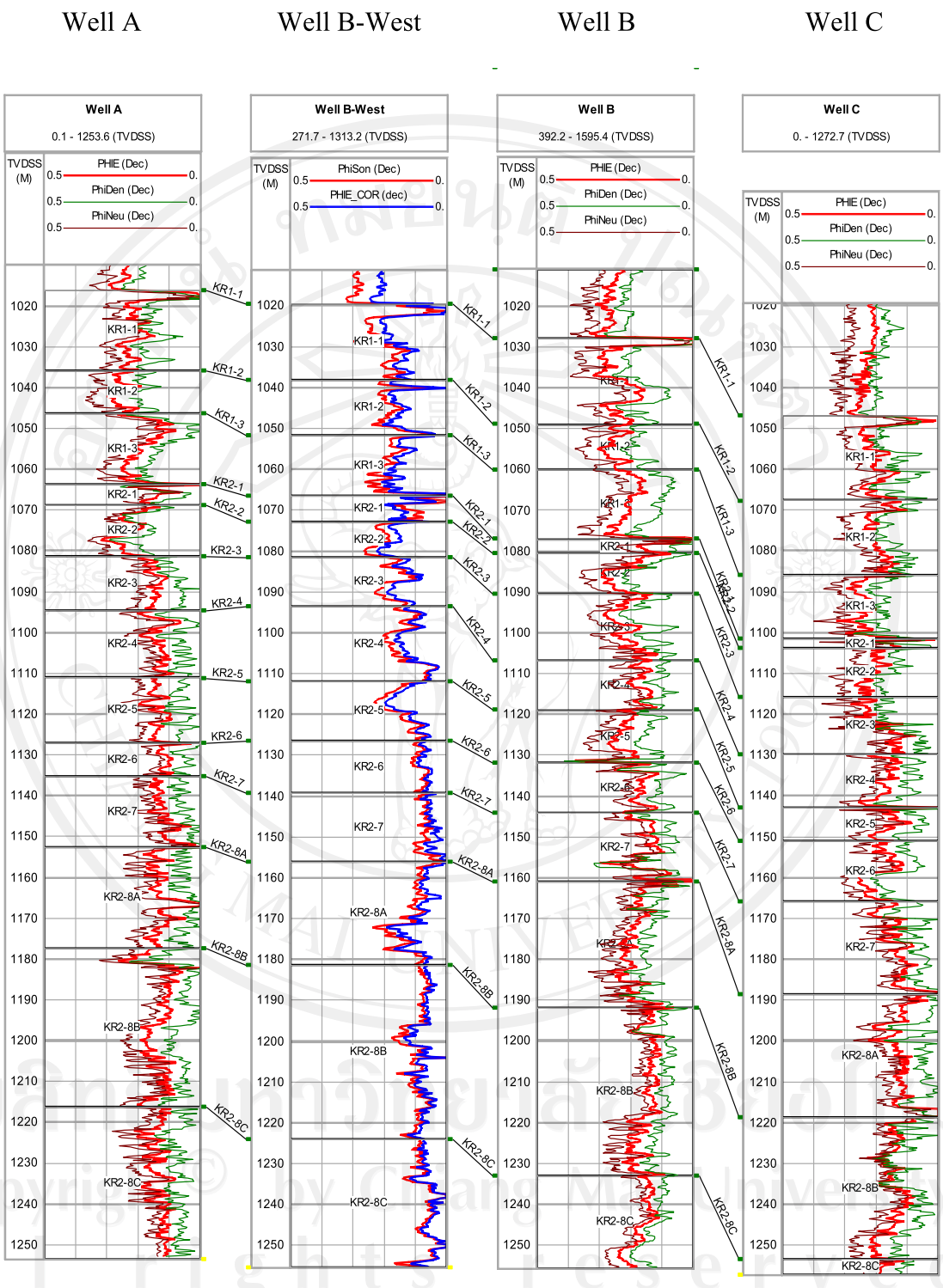

Figure 3.6 Comparison of porosities based on neutron, density (Dewan method, 1983) for well A, well B and well C, and sonic (Wyllie, 1958) for well B-West.

Table 3.3. The average effective porosity (%) by Arithmetic method.

Well	A	B-West	B	C
KR1-1	22	19	24	19
KR1-2	26	18	25	20
KR1-3	19	18	21	24
KR2-1	15	10	20	16
KR2-2	22	21	21	22
KR2-3	16	17	21	18
KR2-4	14	13	17	18
KR2-5	15	14	23	17
KR2-6	13	8	15	18
KR2-7	13	7	16	13
KR2-8A	13	12	19	12
KR2-8B	15	9	15	17

The effective porosity of reservoir units averages at 22% in unit KR1-1 and decreases with burial depth to an average value of 12% in unit KR2-8B (Figure 3.7). The generalized average porosities of reservoir units are summarized below.

- Unit KR1-1, maximum porosity of 24% in well B and average porosity of 20% in other 3 wells.
- Unit KR1-2, the highest porosity value of 26% in well A and minimum value 18% in well B-West.
- Unit KR1-3, maximum 24% in well C and average porosity 19%.
- Unit KR2-1, maximum 20% in well B and minimum value 10% in well B-West.
- Unit KR2-2, average porosity 21% in all wells.
- Unit KR2-3, maximum 21% in well B and average porosity 18%.
- Unit KR2-4, maximum 18% in well C and minimum porosity 13% in well B-West.

- Unit KR2-5, maximum 23% in well B and average porosity 17%.
- Unit KR2-6, maximum 18% in well C and minimum porosity 8% in well B-West.
- Unit KR2-7, maximum 16% in well B and minimum porosity 7% in well B-West.
- Unit KR2-8A, maximum 19% in well B and average porosity 13%.
- Unit KR2-8B, maximum 17% in well C and minimum porosity 9% in well B-West.

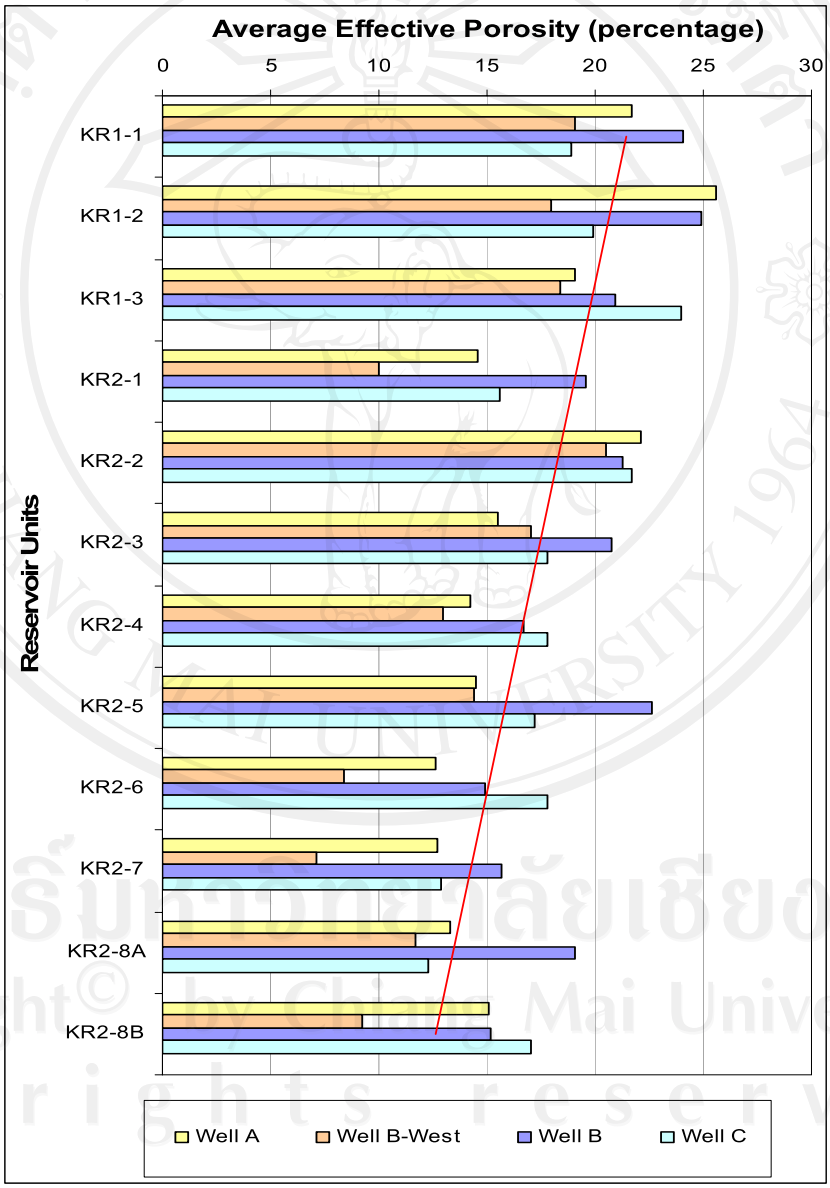

Figure 3.7 Comparison of average effective porosities. Red line indicates the decreasing trend of porosity with burial depth.

3.6 Estimating cementation factor (m) and resistivity of formation water (Rw) using Pickett plot method

The cementation factor is difficult to measure through logging tools. An empirical approach based on resistivity and porosity relations by Pickett plot is the most practical method to estimate these factors using well logs.

Cementation factor is the product of pore networks and agents of cemented material within pores, and type of fluids contained in formation such as water (fresh or saline) and hydrocarbon (oil or gas). The degree of cementation factor varies with relief of pore morphology and nature of pore size network. Larger factor shown in larger pore and it is related to difference in surface relief and pore structures. The cementation factor is around 2. The variation depends on resistivity of formation water with porosity changes. Resistivity of the formation water is a function of the type of fluids (fresh or brine) and temperature of formation, and chiefly related to porosities also.

Although the Pickett plot method is mostly reliable to acquire “m” and “Rw”, there were a number of factors of concerns in shaly sand reservoirs of this study. Then the cementation factors were adjustable with the presence of shale/clay, porosity and type of lithology.

The presented values of “m” and “Rw” associated with depth ranges by Pickett plot were realized and extracted in Figures 3.8 to 3.19. The results were exclusively concentrated to understand the varying “m” with resistivity and porosity for studied formations.

Summary of cementation factor and resistivity of water by Pickett plot were listed in Table 3.4.

Table 3.4. Summary of cementation factor and resistivity of formation water by Pickett plot method.

Well	Reservoir Unit	Ranged on Pickett plot From	To	m	Rw
A	KR1-1	1183	1187	2.05	1.08
B-West		1087	1088.5	2.58	0.75
B		1046	1049	2.04	1.17
C		1318	1323	3.40	0.73
A	KR1-2	1205	1211	2.04	1.00
B-West		1102	1105	2.10	0.71
B		1061	1068	1.90	0.66
C		1345	1350	2.00	1.47
A	KR1-3	1226	1231	2.02	1.11
B-West		1115.4	1116.8	2.78	0.19
B		1075	1082	2.30	0.45
C		1371	1373	1.30	2.22
A	KR2-1	1238	1241.2	2.10	0.35
B-West		1124	1125	1.92	0.45
B		1087	1089	2.23	0.45
C		1374	1376	1.86	0.91
A	KR2-2	1251	1287	2.17	2.43
B-West		1136	1139	2.94	0.52
B		1093	1097	2.16	0.99
C		1377	1382	1.96	0.81
A	KR2-3	1263	1267	2.38	0.80
B-West		1145	1146	1.78	2.10
B		1109	1113	2.55	0.68
C		1404	1409	2.41	0.36
A	KR2-4	1287	1296	2.24	0.599
B-West		1168	1173	1.93	0.654
B		1123	1127	2.15	1.01
C		1418	1419	2.01	1.16
A	KR2-5	1305	1312	2.16	0.665
B-West		1175	1180	3.08	0.378
B		1130.2	1132.6	2.13	0.71
C		1437	1439	1.90	0.612
A	KR2-6	1320	1327	1.95	0.75
B-West		1199.8	1202	1.57	1.48
B		1151	1153	1.86	1.08
C		1450	1453	2.36	0.46
A	KR2-7	1333	1345	2.04	0.47
B-West		1205.5	1208	2.32	0.32
B		1153	1170	1.93	0.75
C		1484	1492	1.97	0.98
A	KR2-8A	1374	1376	1.89	0.41
B-West		1233	1239	1.92	0.70
B		1195	1198	2.17	0.85
C		1524	1525	1.89	0.65
A	KR2-8B	1421	1429	1.69	0.91
B-West		1272	1279	2.39	0.18
B		1218	1226	2.02	0.74
C		1545	1553	1.93	0.68
Arithmetic Mean				**2.13**	**0.82**

As per analyzing the “m” values by Pickett plot, it was concluded that reservoir units compiles with the “m” values of Humble formula for unconsolidated sands (Tertiary). Since the study area is composed of upper Oligocene-Miocene alluvial/fluvial deposits, the Humble formula is proper to be applied in water saturation models afterward.

$F = 0.62/\phi^{2.15}$ Humble formula for unconsolidated sands (Tertiary)

where 0.62 for “a” Tortuosity or porosity factor

2.15 for “m” cementation factor.

The estimated “Rw” values by Pickett plot were initially exercised in shaly sand water saturation models. These were recalibrated under saturation models and fixed into the reservoir units related to deep resistivity (LLD) and shallow resistivity (LLS or MSFL).

Figure 3.8 to Figure 3.9 illustrate the Picket plots of reservoir units for studied wells. The conclusive values of “Rw” after the recalibration under saturation models are listed in Table 3.5.

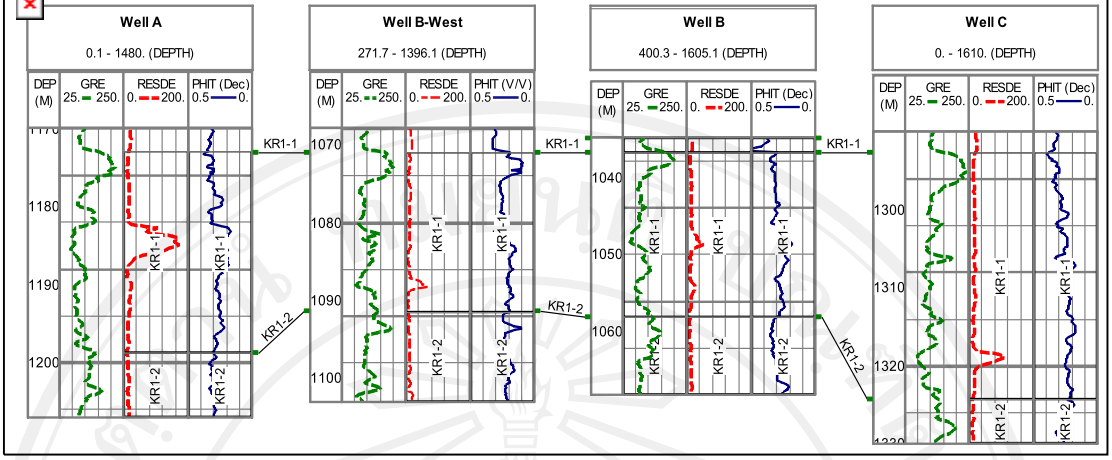

(a) Unit KR1-1, correlation with GR, Rt and PHIT

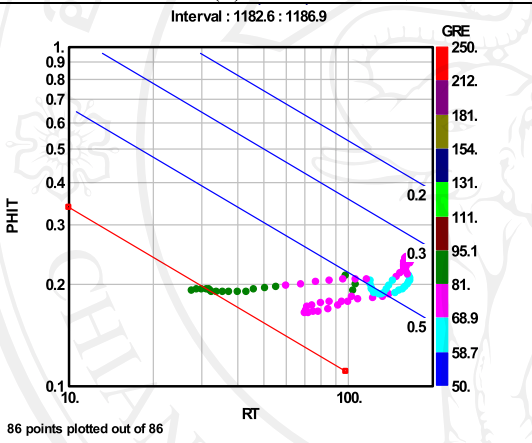

(b) Well A, unit KR1-1
Depth 1183-1187 mMD
m 2.05, Rw 1.08

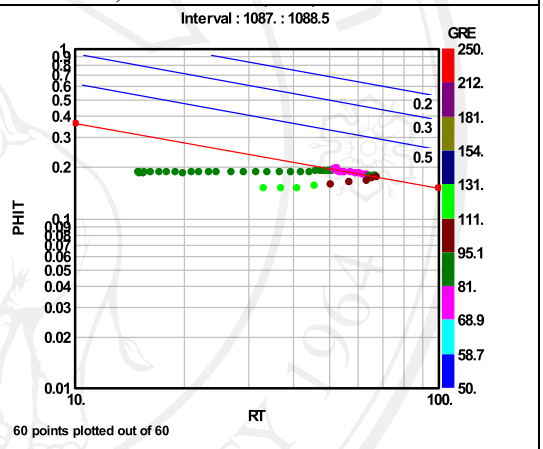

(c) Well B-West, unit KR1-1
Depth 1087-1088.5 mMD
m 2.58, Rw 0.75

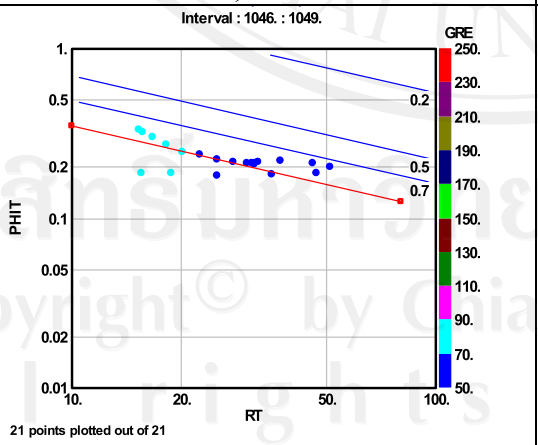

(d) Well B, unit KR1-1
Depth 1046-1049 mMD
m 2.04, Rw 1.17

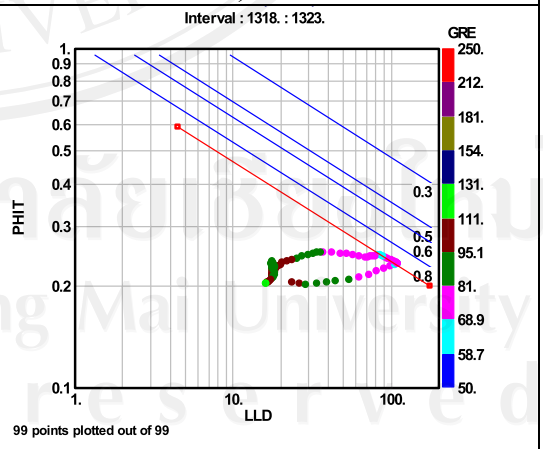

(e) Well C, unit KR1-1
Depth 1318-1323 mMD
m 3.4, Rw 0.733

Figure 3.8 Pickett plot of unit KR1-1 of well A, B-West, B, and C, Figure (a) flattened to top of KR1-1.

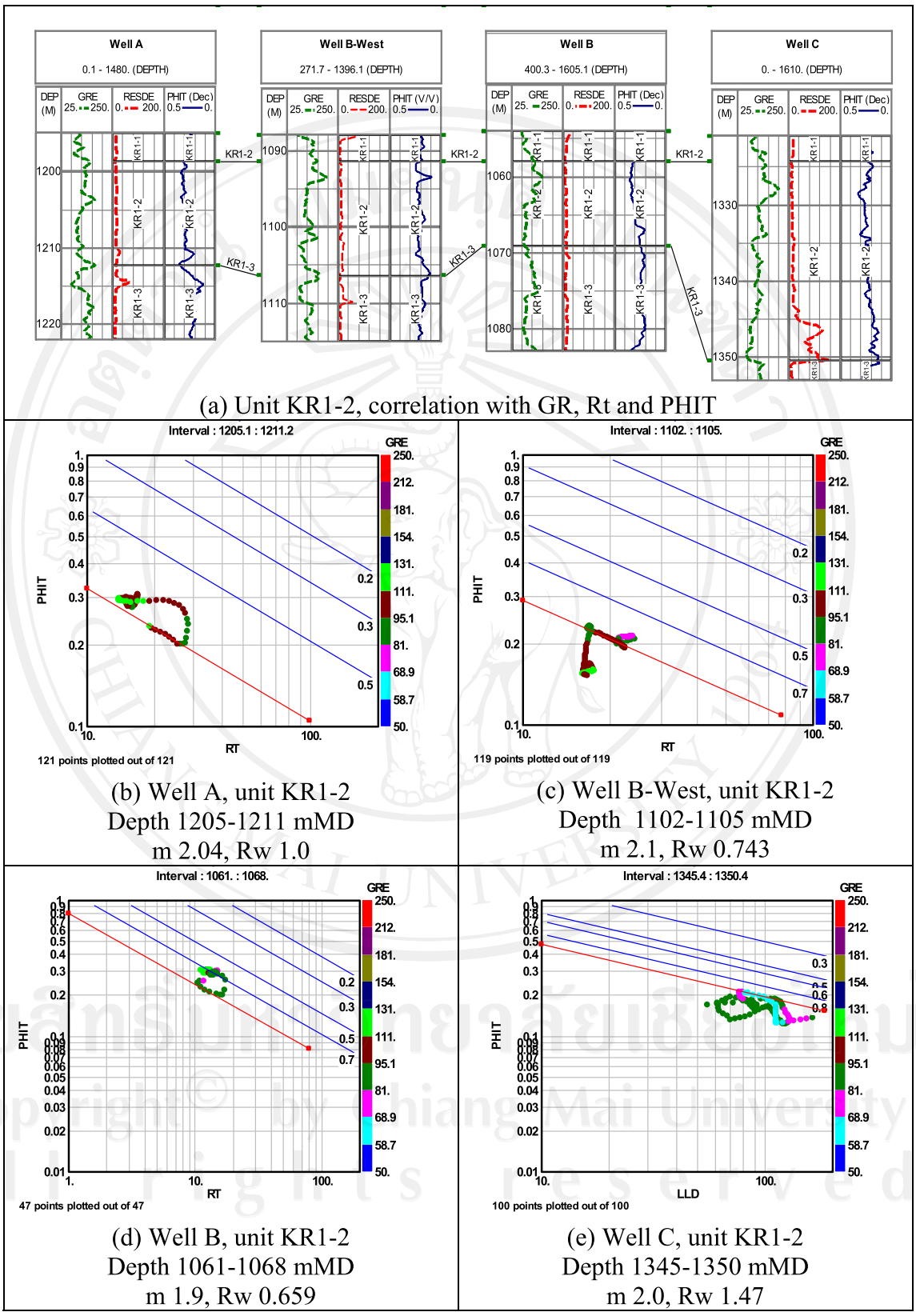

(a) Unit KR1-2, correlation with GR, Rt and PHIT

(b) Well A, unit KR1-2
Depth 1205-1211 mMD
m 2.04, Rw 1.0

(c) Well B-West, unit KR1-2
Depth 1102-1105 mMD
m 2.1, Rw 0.743

(d) Well B, unit KR1-2
Depth 1061-1068 mMD
m 1.9, Rw 0.659

(e) Well C, unit KR1-2
Depth 1345-1350 mMD
m 2.0, Rw 1.47

Figure 3.9 Pickett plot of unit KR1-2 of well A, B-West, B, and C, Figure (a) flattened to top of KR1-2.

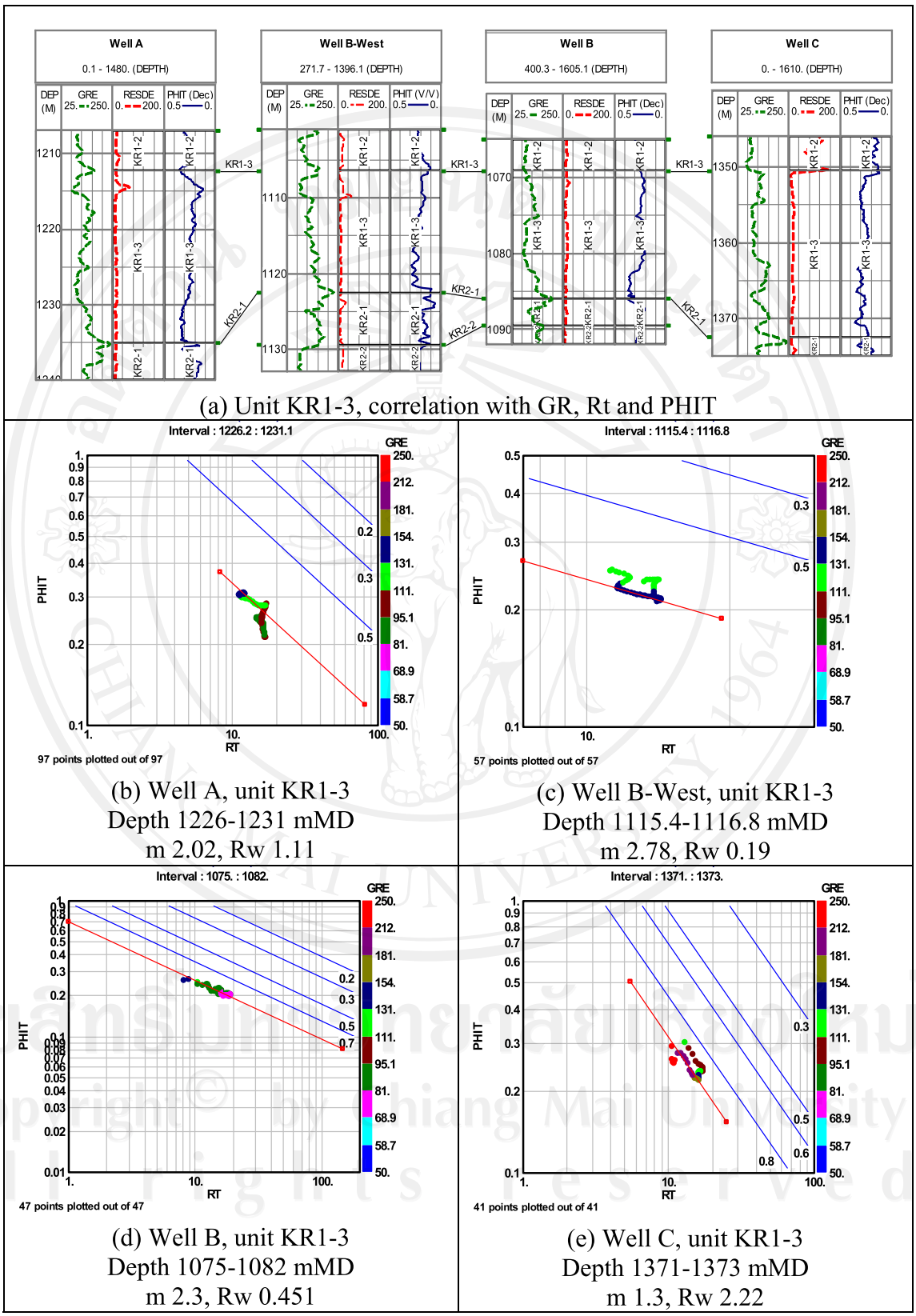

(a) Unit KR1-3, correlation with GR, Rt and PHIT

(b) Well A, unit KR1-3
Depth 1226-1231 mMD
m 2.02, Rw 1.11

(c) Well B-West, unit KR1-3
Depth 1115.4-1116.8 mMD
m 2.78, Rw 0.19

(d) Well B, unit KR1-3
Depth 1075-1082 mMD
m 2.3, Rw 0.451

(e) Well C, unit KR1-3
Depth 1371-1373 mMD
m 1.3, Rw 2.22

Figure 3.10 Pickett plot of unit KR1-3 of well A, B-West, B, and C, Figure (a) flattened to top of KR1-3.

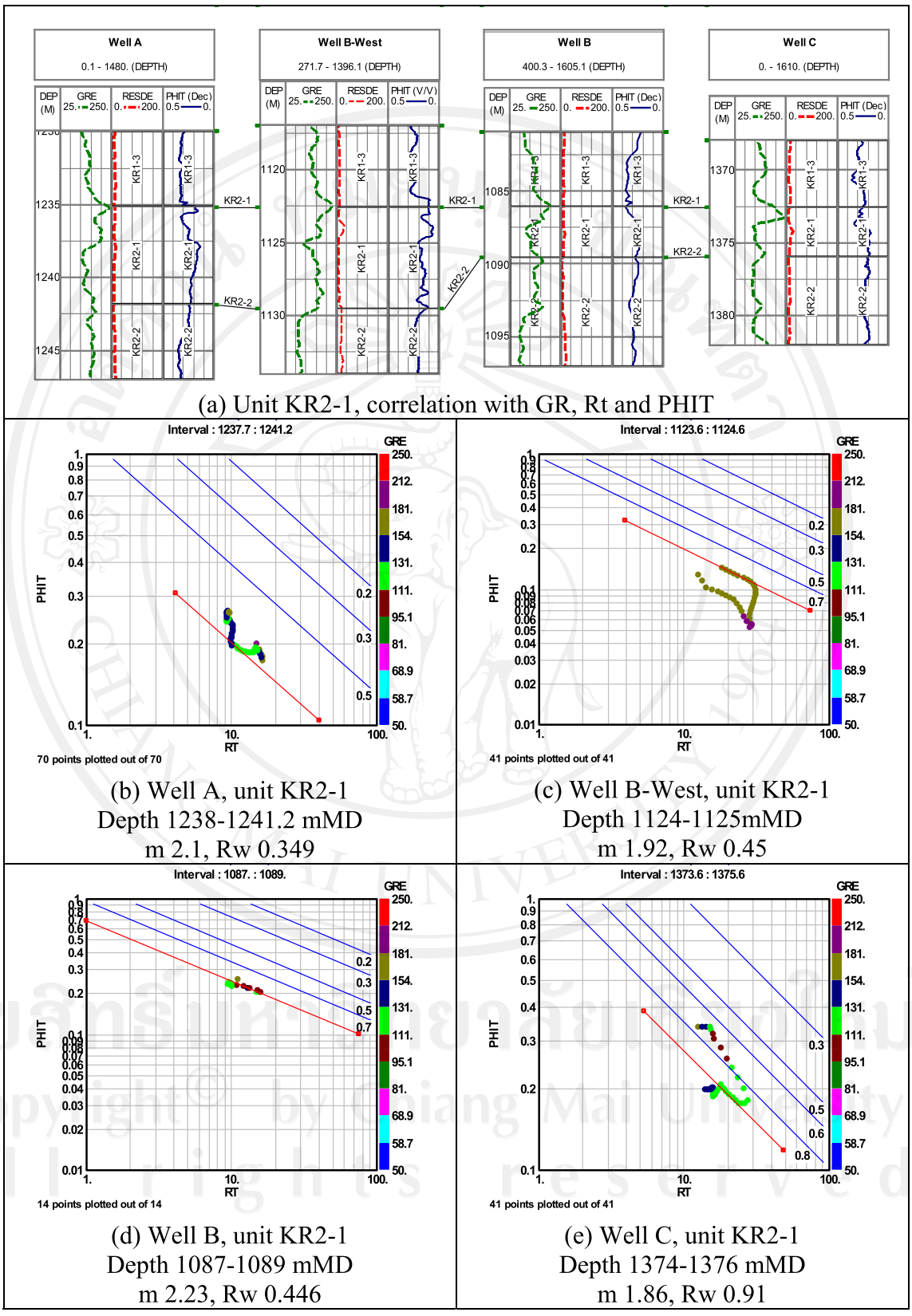

(a) Unit KR2-1, correlation with GR, Rt and PHIT

(b) Well A, unit KR2-1
Depth 1238-1241.2 mMD
m 2.1, Rw 0.349

(c) Well B-West, unit KR2-1
Depth 1124-1125mMD
m 1.92, Rw 0.45

(d) Well B, unit KR2-1
Depth 1087-1089 mMD
m 2.23, Rw 0.446

(e) Well C, unit KR2-1
Depth 1374-1376 mMD
m 1.86, Rw 0.91

Figure 3.11 Pickett plot of unit KR2-1 of well A, B-West, B, and C, Figure (a) flattened to top of KR2-1.

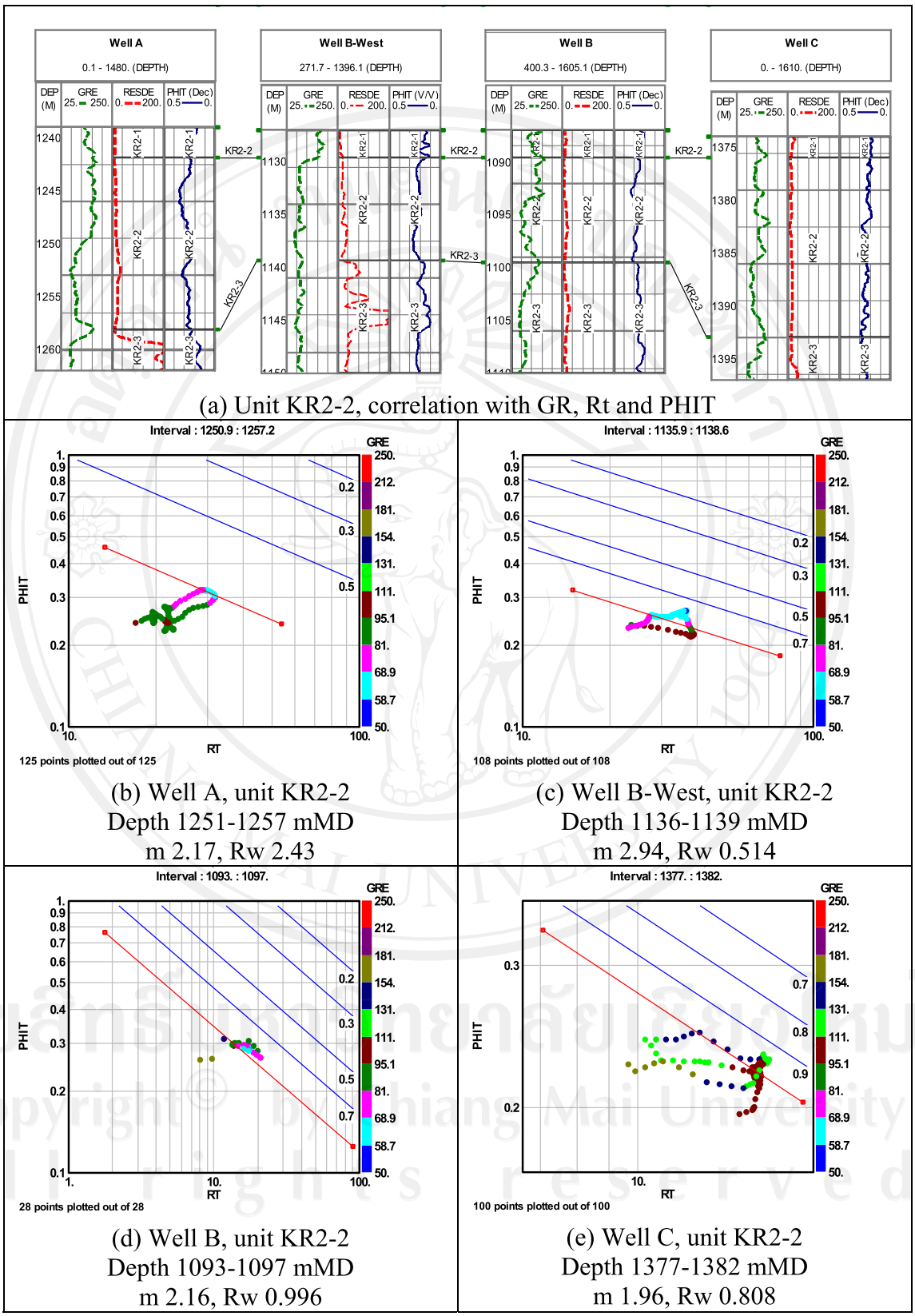

(a) Unit KR2-2, correlation with GR, Rt and PHIT

(b) Well A, unit KR2-2
Depth 1251-1257 mMD
m 2.17, Rw 2.43

(c) Well B-West, unit KR2-2
Depth 1136-1139 mMD
m 2.94, Rw 0.514

(d) Well B, unit KR2-2
Depth 1093-1097 mMD
m 2.16, Rw 0.996

(e) Well C, unit KR2-2
Depth 1377-1382 mMD
m 1.96, Rw 0.808

Figure 3.12 Pickett plot of unit KR2-2 of well A, B-West, B, and C, Figure (a) flattened to top of KR2-2.

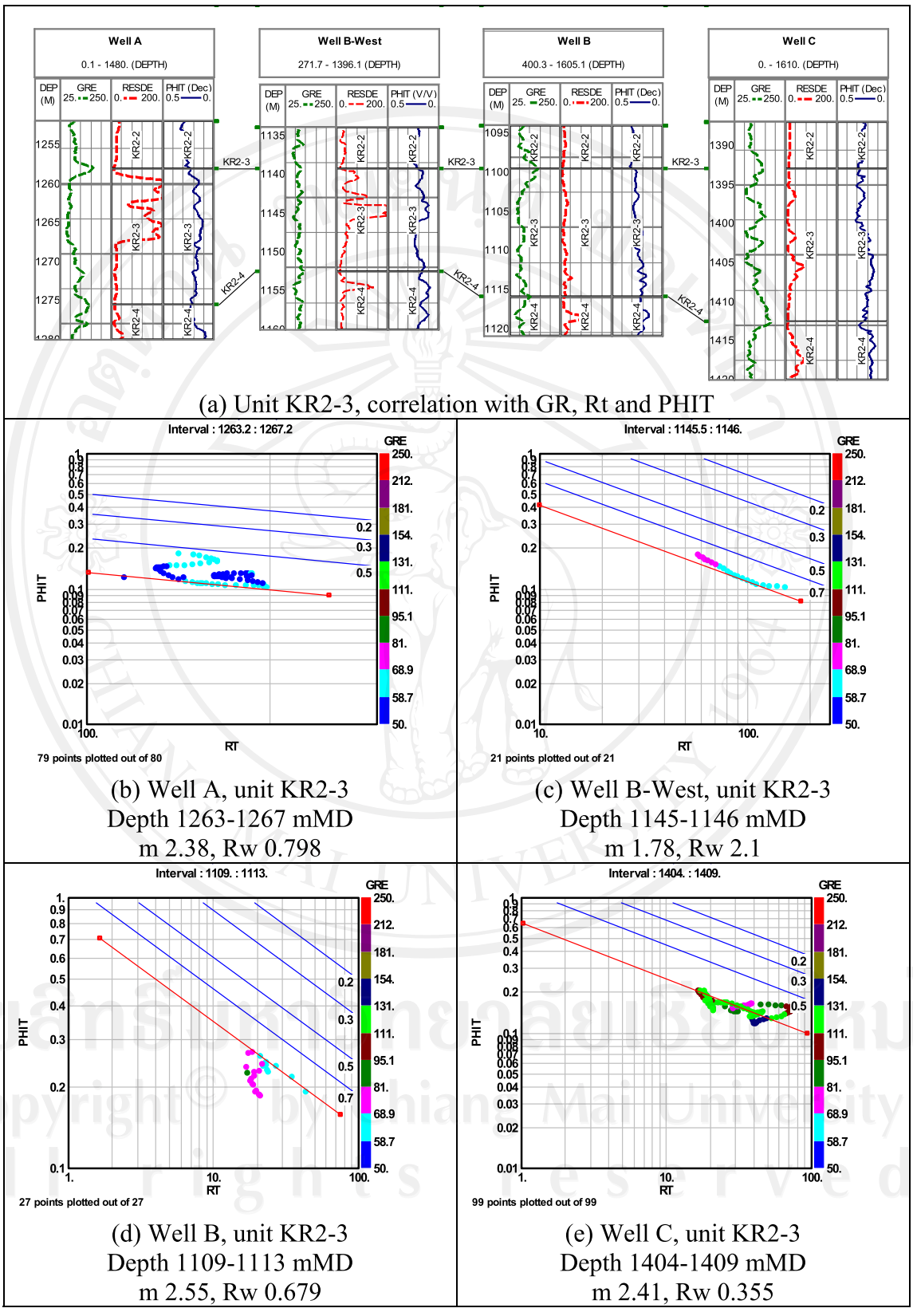

(a) Unit KR2-3, correlation with GR, Rt and PHIT

(b) Well A, unit KR2-3
Depth 1263-1267 mMD
m 2.38, Rw 0.798

(c) Well B-West, unit KR2-3
Depth 1145-1146 mMD
m 1.78, Rw 2.1

(d) Well B, unit KR2-3
Depth 1109-1113 mMD
m 2.55, Rw 0.679

(e) Well C, unit KR2-3
Depth 1404-1409 mMD
m 2.41, Rw 0.355

Figure 3.13 Pickett plot of unit KR2-3 of well A, B-West, B, and C, Figure (a) flattened to top of KR2-3.

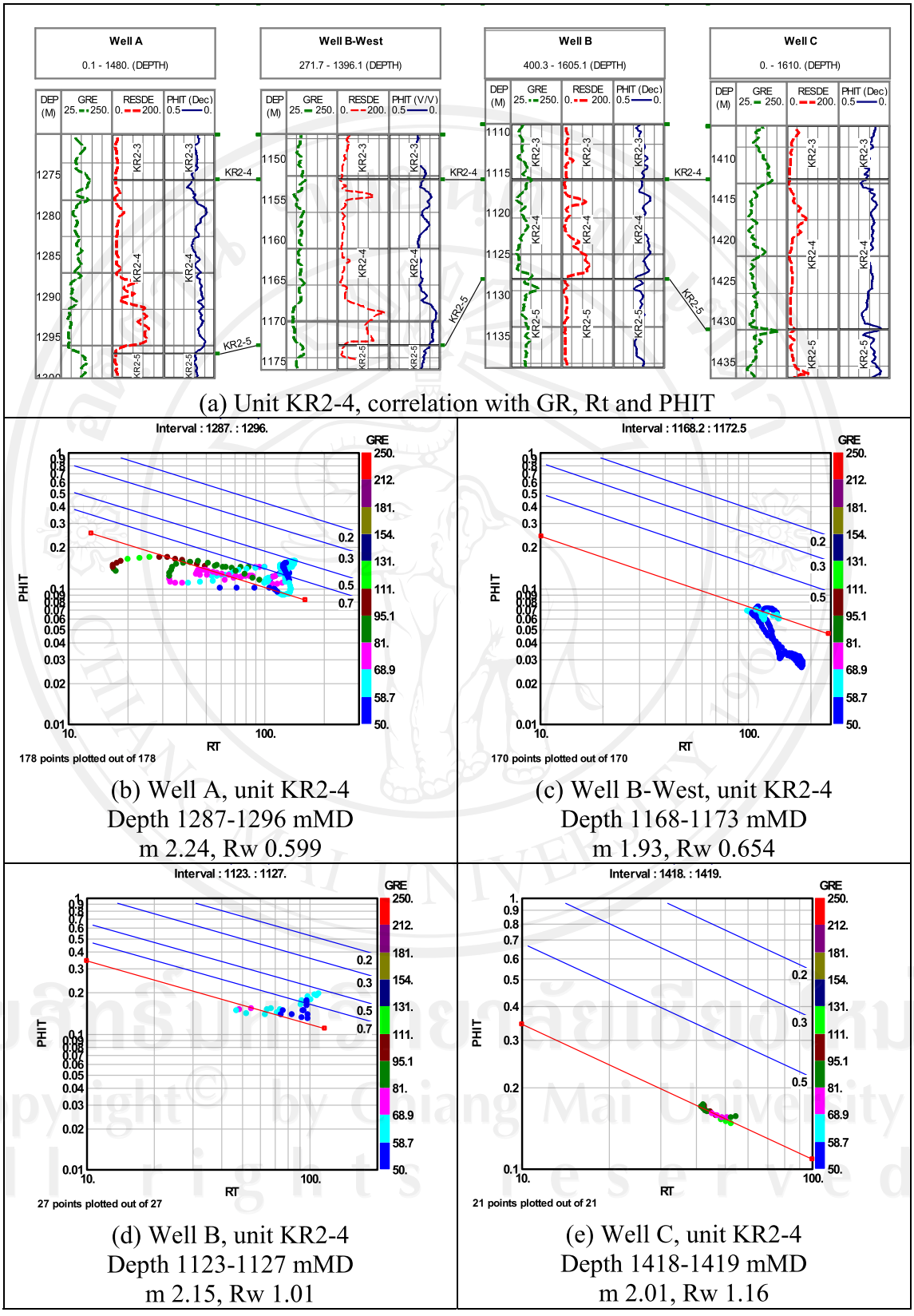

(a) Unit KR2-4, correlation with GR, Rt and PHIT

(b) Well A, unit KR2-4
Depth 1287-1296 mMD
m 2.24, Rw 0.599

(c) Well B-West, unit KR2-4
Depth 1168-1173 mMD
m 1.93, Rw 0.654

(d) Well B, unit KR2-4
Depth 1123-1127 mMD
m 2.15, Rw 1.01

(e) Well C, unit KR2-4
Depth 1418-1419 mMD
m 2.01, Rw 1.16

Figure 3.14 Pickett plot of unit KR2-4 of well A, B-West, B, and C, Figure (a) flattened to top of KR2-4.

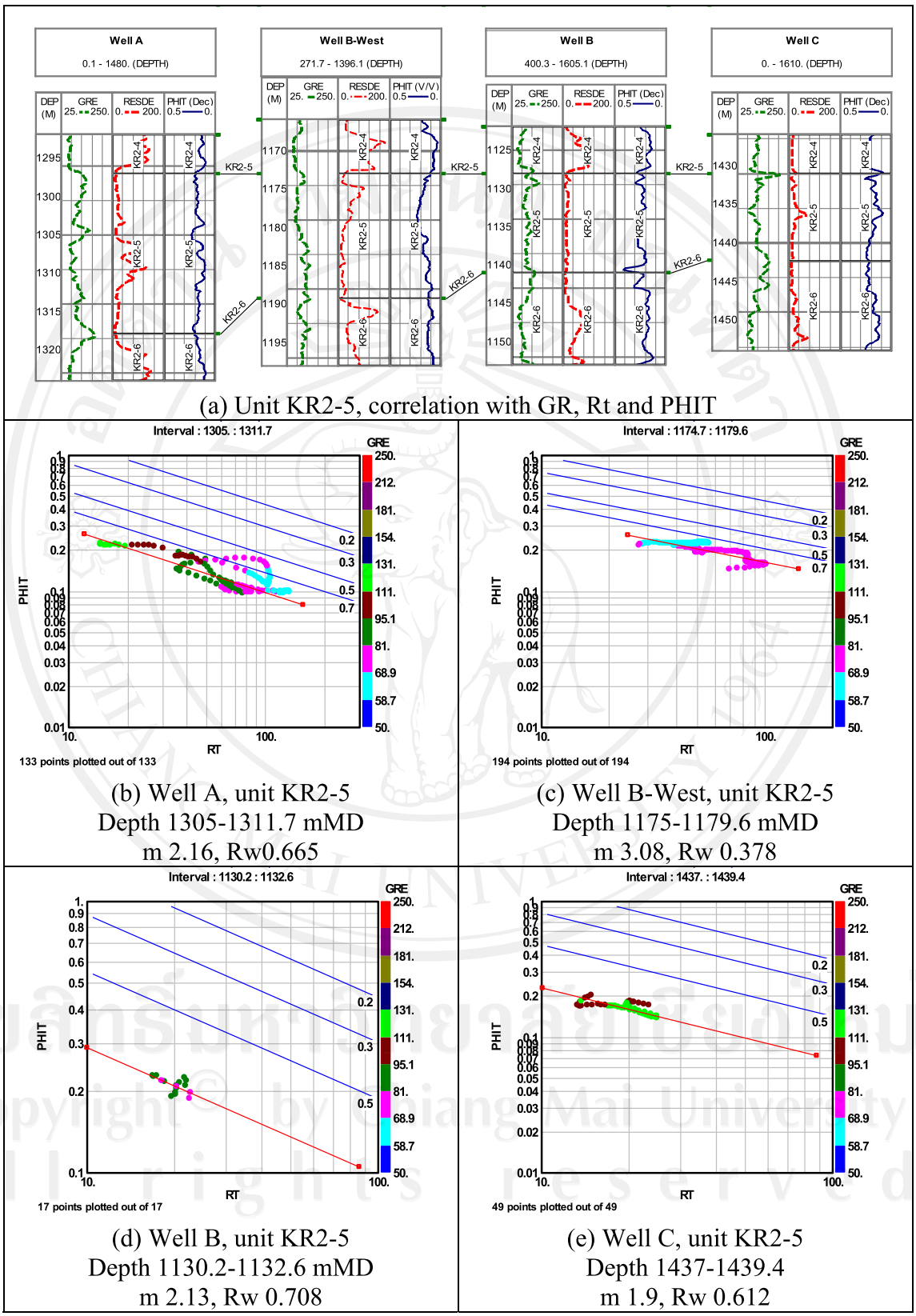

(a) Unit KR2-5, correlation with GR, Rt and PHIT

(b) Well A, unit KR2-5
Depth 1305-1311.7 mMD
m 2.16, Rw0.665

(c) Well B-West, unit KR2-5
Depth 1175-1179.6 mMD
m 3.08, Rw 0.378

(d) Well B, unit KR2-5
Depth 1130.2-1132.6 mMD
m 2.13, Rw 0.708

(e) Well C, unit KR2-5
Depth 1437-1439.4
m 1.9, Rw 0.612

Figure 3.15 Pickett plot of unit KR2-5 of well A, B-West, B, and C, Figure (a) flattened to top of KR2-5.

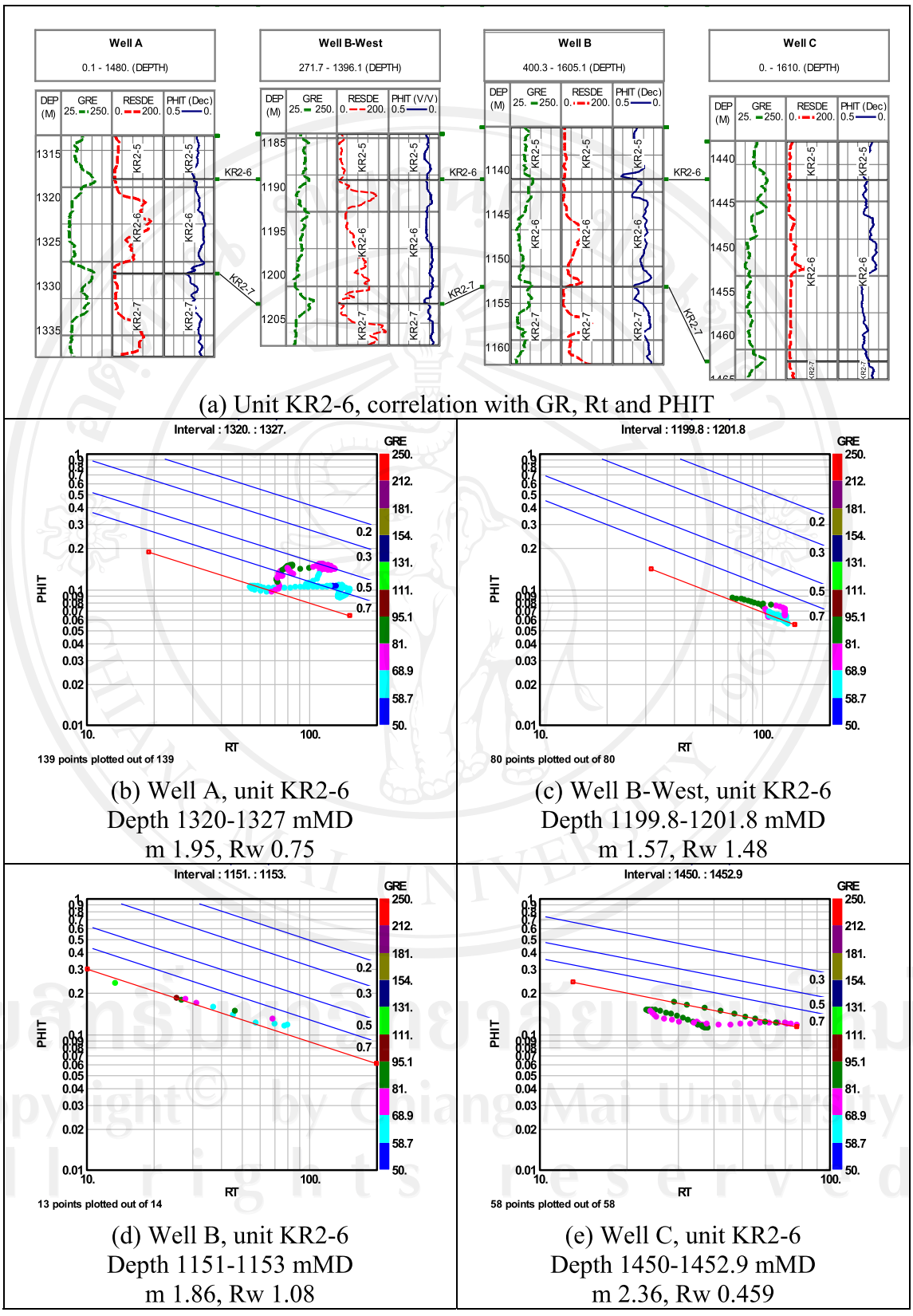

(a) Unit KR2-6, correlation with GR, Rt and PHIT

(b) Well A, unit KR2-6
Depth 1320-1327 mMD
m 1.95, Rw 0.75

(c) Well B-West, unit KR2-6
Depth 1199.8-1201.8 mMD
m 1.57, Rw 1.48

(d) Well B, unit KR2-6
Depth 1151-1153 mMD
m 1.86, Rw 1.08

(e) Well C, unit KR2-6
Depth 1450-1452.9 mMD
m 2.36, Rw 0.459

Figure 3.16 Pickett plot of unit KR2-6 of well A, B-West, B, and C, Figure (a) flattened to top of KR2-6.

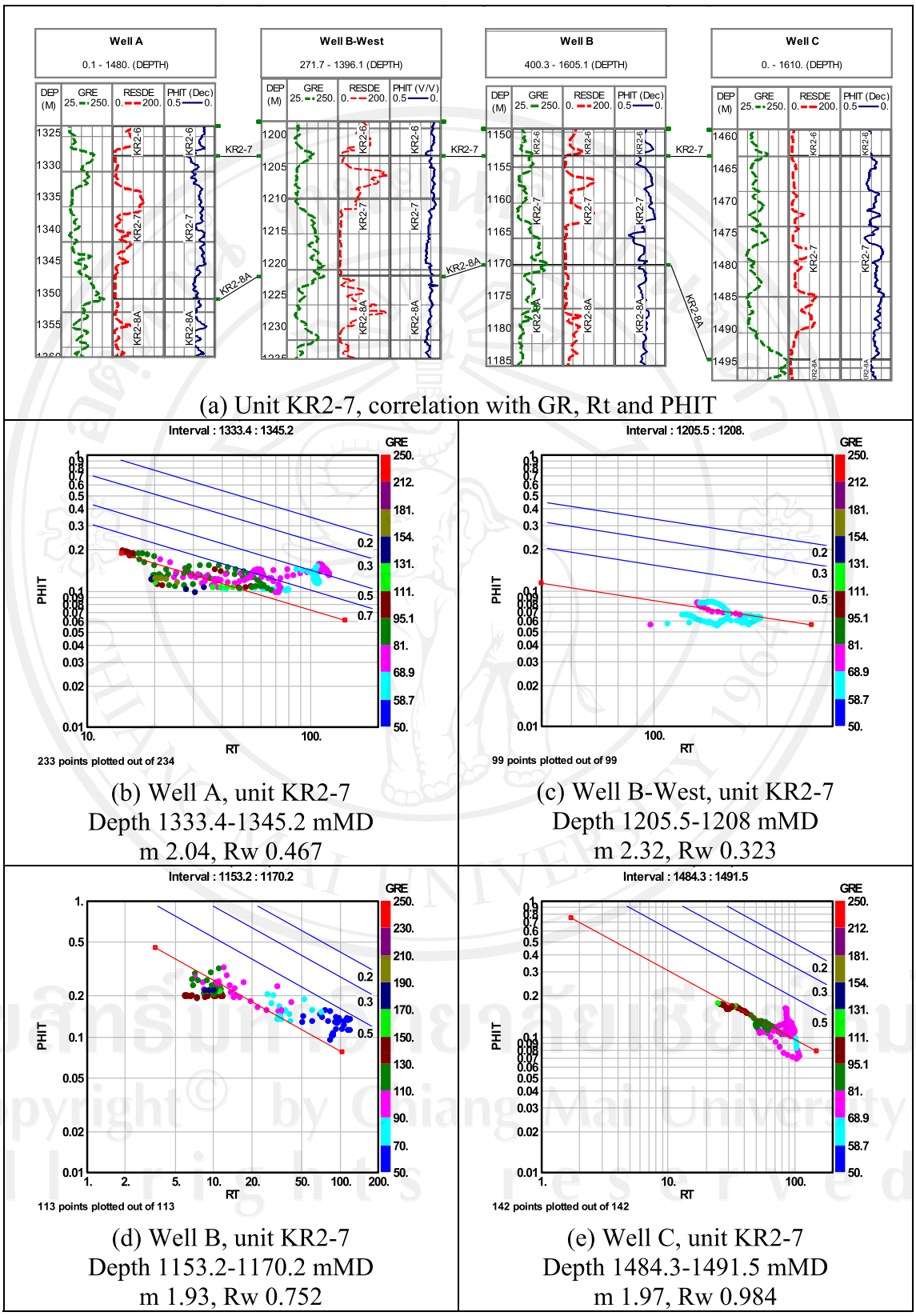

(a) Unit KR2-7, correlation with GR, Rt and PHIT

(b) Well A, unit KR2-7
Depth 1333.4-1345.2 mMD
m 2.04, Rw 0.467

(c) Well B-West, unit KR2-7
Depth 1205.5-1208 mMD
m 2.32, Rw 0.323

(d) Well B, unit KR2-7
Depth 1153.2-1170.2 mMD
m 1.93, Rw 0.752

(e) Well C, unit KR2-7
Depth 1484.3-1491.5 mMD
m 1.97, Rw 0.984

Figure 3.17 Pickett plot of unit KR2-7 of well A, B-West, B, and C, Figure (a) flattened to top of KR2-7.

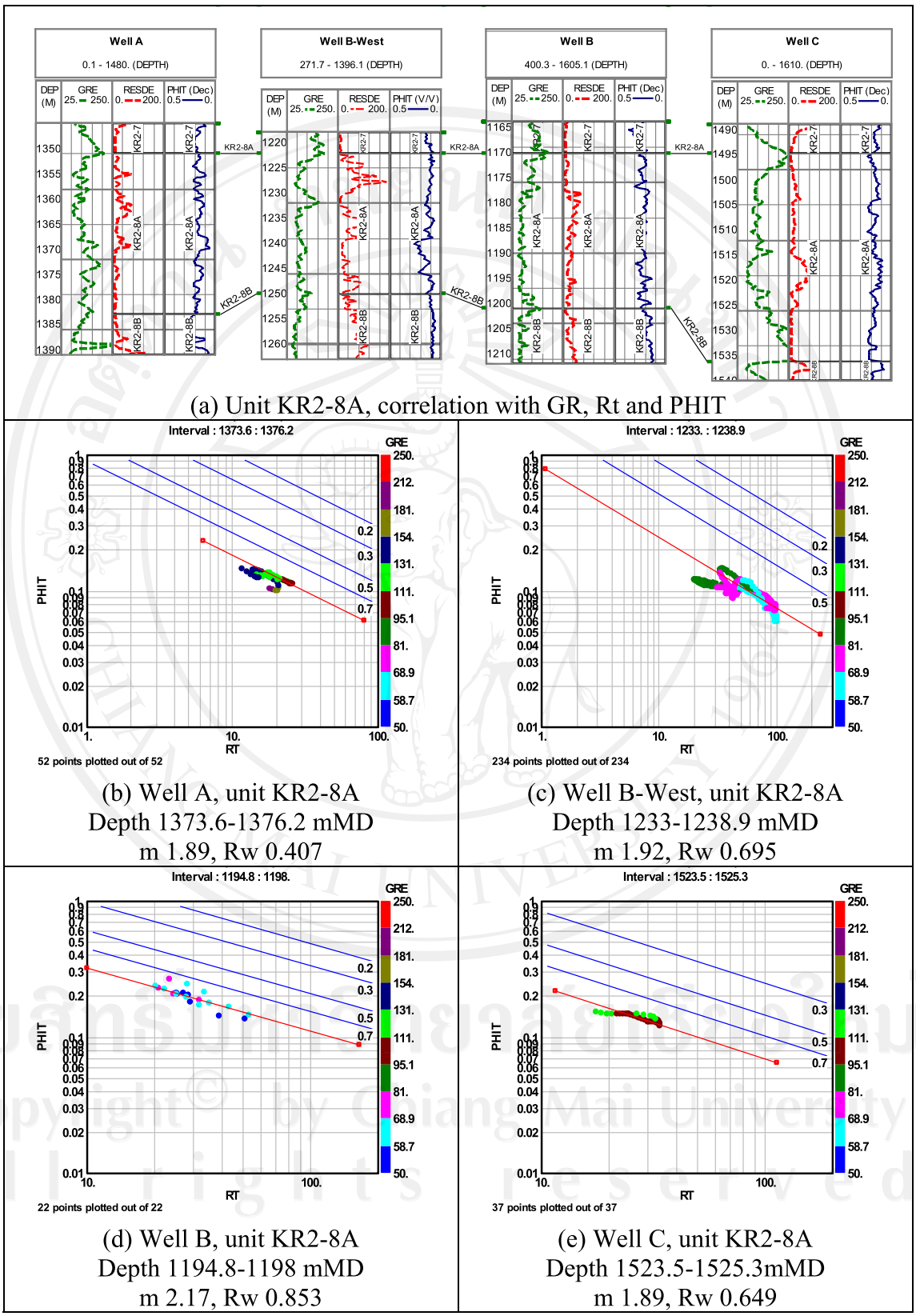

(a) Unit KR2-8A, correlation with GR, Rt and PHIT

(b) Well A, unit KR2-8A
Depth 1373.6-1376.2 mMD
m 1.89, Rw 0.407

(c) Well B-West, unit KR2-8A
Depth 1233-1238.9 mMD
m 1.92, Rw 0.695

(d) Well B, unit KR2-8A
Depth 1194.8-1198 mMD
m 2.17, Rw 0.853

(e) Well C, unit KR2-8A
Depth 1523.5-1525.3mMD
m 1.89, Rw 0.649

Figure 3.18 Pickett plot of unit KR2-8A of well A, B-West, B, and C, Figure (a) flattened to top of KR2-8A.

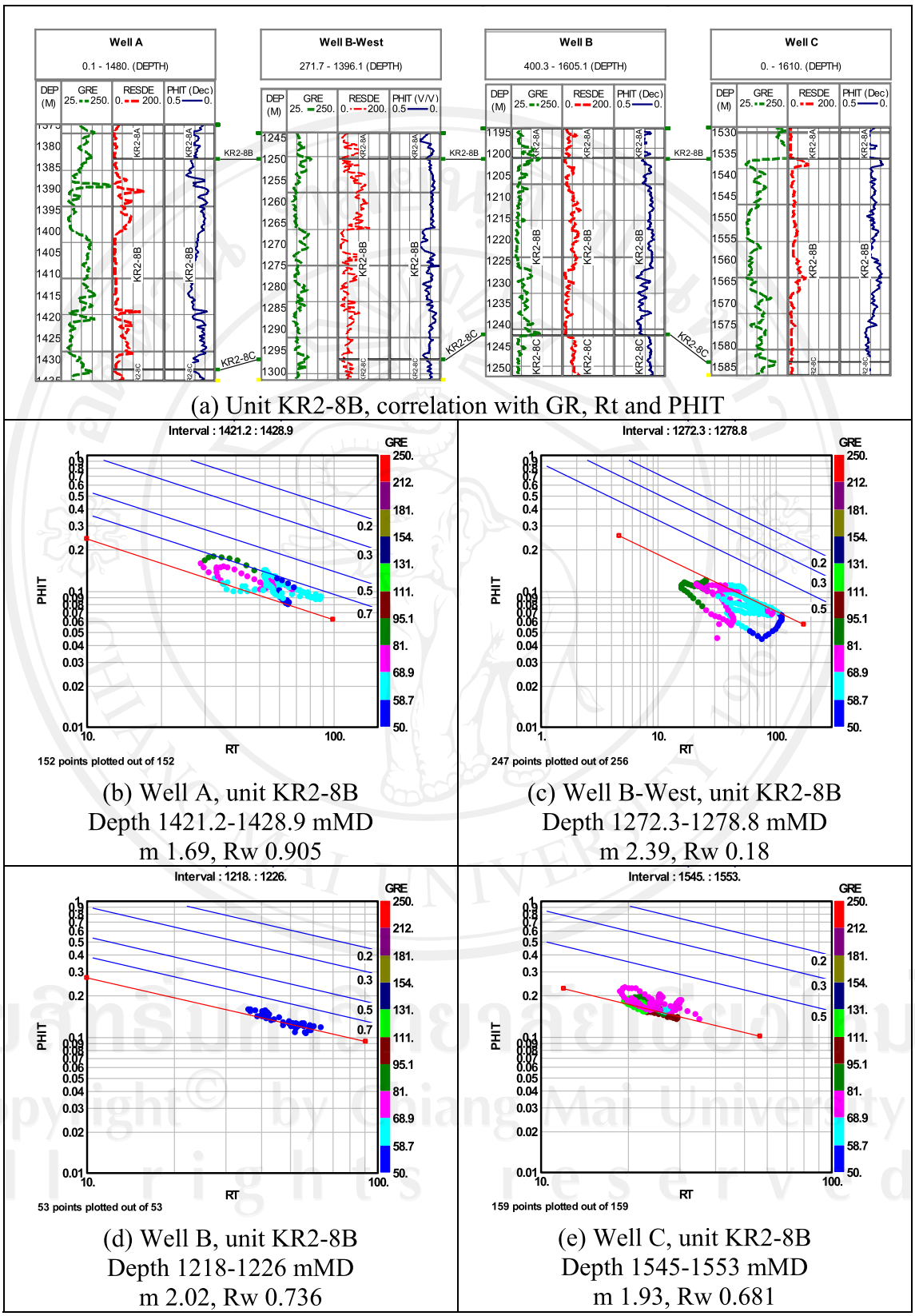

(a) Unit KR2-8B, correlation with GR, Rt and PHIT

(b) Well A, unit KR2-8B
Depth 1421.2-1428.9 mMD
m 1.69, Rw 0.905

(c) Well B-West, unit KR2-8B
Depth 1272.3-1278.8 mMD
m 2.39, Rw 0.18

(d) Well B, unit KR2-8B
Depth 1218-1226 mMD
m 2.02, Rw 0.736

(e) Well C, unit KR2-8B
Depth 1545-1553 mMD
m 1.93, Rw 0.681

Figure 3.19 Pickett plot of unit KR2-8B of well A, B-West, B, and C, Figure (a) flattened to top of KR2-8B.

Table 3.5 Recalibrated Rw values under shaly sand water saturation models.

Reservoir Unit	Well	Recalibrated "Rw"
KR1-1	A	1.20
	B-West	0.83
	B	1.10
	C	0.80
KR1-2	A	1.60
	B-West	0.60
	B	1.10
	C	1.00
KR1-3	A	1.10
	B-West	0.62
	B	0.85
	C	1.10
KR2-1	A	0.95
	B-West	0.63
	B	0.80
	C	1.10
KR2-2	A	1.40
	B-West	1.00
	B	1.00
	C	0.80
KR2-3	A	1.10
	B-West	1.20
	B	0.72
	C	0.80
KR2-4	A	0.87
	B-West	0.83
	B	0.98
	C	0.70
KR2-5	A	0.70
	B-West	0.60
	B	0.72
	C	0.57
KR2-6	A	0.66
	B-West	0.43
	B	0.97
	C	0.56
KR2-7	A	0.63
	B-West	0.37
	B	0.80
	C	0.70
KR2-8A	A	0.55
	B-West	0.54
	B	0.96
	C	0.70
KR2-8B	A	1.30
	B-West	0.37
	B	0.80
	C	0.82

3.7 Estimating of Water Saturation (Sw)

The different variety of water saturation methods are practically used for the evaluation of shaly sand models. Poupon (1954) modified the Archie's equation used specifically in laminated shale formation with the definition of resistivity. He considered the volume of laminated shale (Vsh) and classified the bound water and free water as a dual-water principle. The shaly sand water saturation models are more developed under the investigation with conductivity (reciprocal of resistivity) of formation and fluid contents.

Conductivity (C) is reciprocal to resistivity and is expressed in millimhos per meter (mmho/m). The conductivity is often exceptionally large relative to the amount of shale in shaly sand formation (Schlumberger, 1989). Figure 3.20 explains the relationship between conductivity of water and oil in clean formation and, variation of their correlation with magnitude of shaliness.

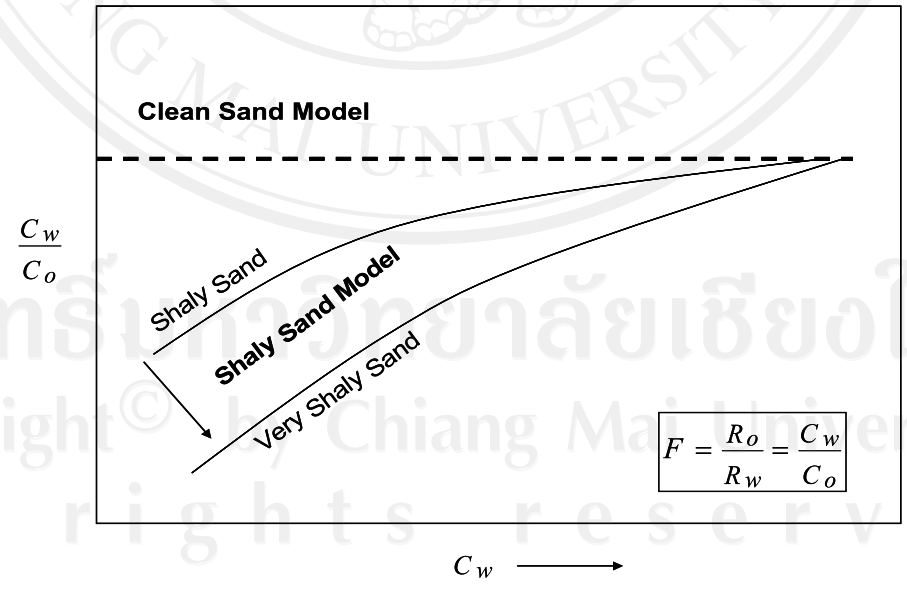

Figure 3.20 Clean Sand Model and Shaly Sand Models, variation of the ratio of conductivity of water (Cw) and conductivity of oil (Co), with conductivity of water in shaly sands, F= formation factor (Worthington, 1985).

The plots of Cw/Co vs. Cw for clean sand sample provide a straight line (constant value of Cw/Co with varying Cw) parallel to the Cw axis. However, shaly sand formation is not always the constant line and it show decrease of Cw/Co with decreasing Cw (Patnode and Wyllie, 1950). There were other established models with their specific objectives depending on types of shale/clay.

The water saturation models were applied and compared between Archie's model (1941) and populated shaly sand and dual water models. Simandoux (1963) shaly sand model presented only a linear relationship of Cw and Co. The method predicts a decreasing shale effect that is normally applied in low values of water saturation and high shale fractions**.** Modified Simandoux model (Bardon and Pied, 1969) is favorable to estimate the values of formation water saturation above the irreducible water.

Poupon-Leveaux (1971) proposed the "Indonesia formula" an expression with volume of shale (Vsh). This equation is effective in comparatively fresh formation waters and high degrees of shaliness (Vsh<50%). The equation accommodates the non-linear relationship of Cw and Co.

Dual Water Model (Tepper, 1989) was mainly developed with experimentation of laminated shale models related to the free fluid porosity.

To estimate the water saturation by means of shaly sand models, the following methods and factors will be interpolated to fix these models.

- The volume of shale (Vsh) using gamma ray by Clavier method.
- The effective porosity (ϕ_e), neutron-density by Dewan's method (for wells A, B and C).
- Sonic porosity by Wyllie's method (for well B-West only).

- The cementation factor (m) 2.15 and porosity factor (a) 0.62 by Humble formula.

Fundamental problems of the saturation calculations are the uncertainties of formation water resistivity (Rw). Estimated Rw values by Pickett plot method were initially applied in representative zones. The values were subsequently calibrated for the response of formation resistivity (deep and shallow) interfacing with gamma ray, neutron and density relatively.

The estimated water saturation results of the shaly sand models were compared to a dual water model (Figure 3.21). Table 3.6 lists the Arithmetic average of Sw values for each zone. The dual water saturation gives notably smaller values than others figures. The water saturation by Archie's formula provides results of maximum values.

These models could be expressed on the word of mathematic expression below.

$$Sw_{Archie} > Sw_{Sim} > Sw_{Mod.Sim} \geq Sw_{Indo} > Sw_{DW}$$

In accordance with these results of shaly sand models, dual water saturation model is more desirable to determine the Sw in these potential reservoirs.

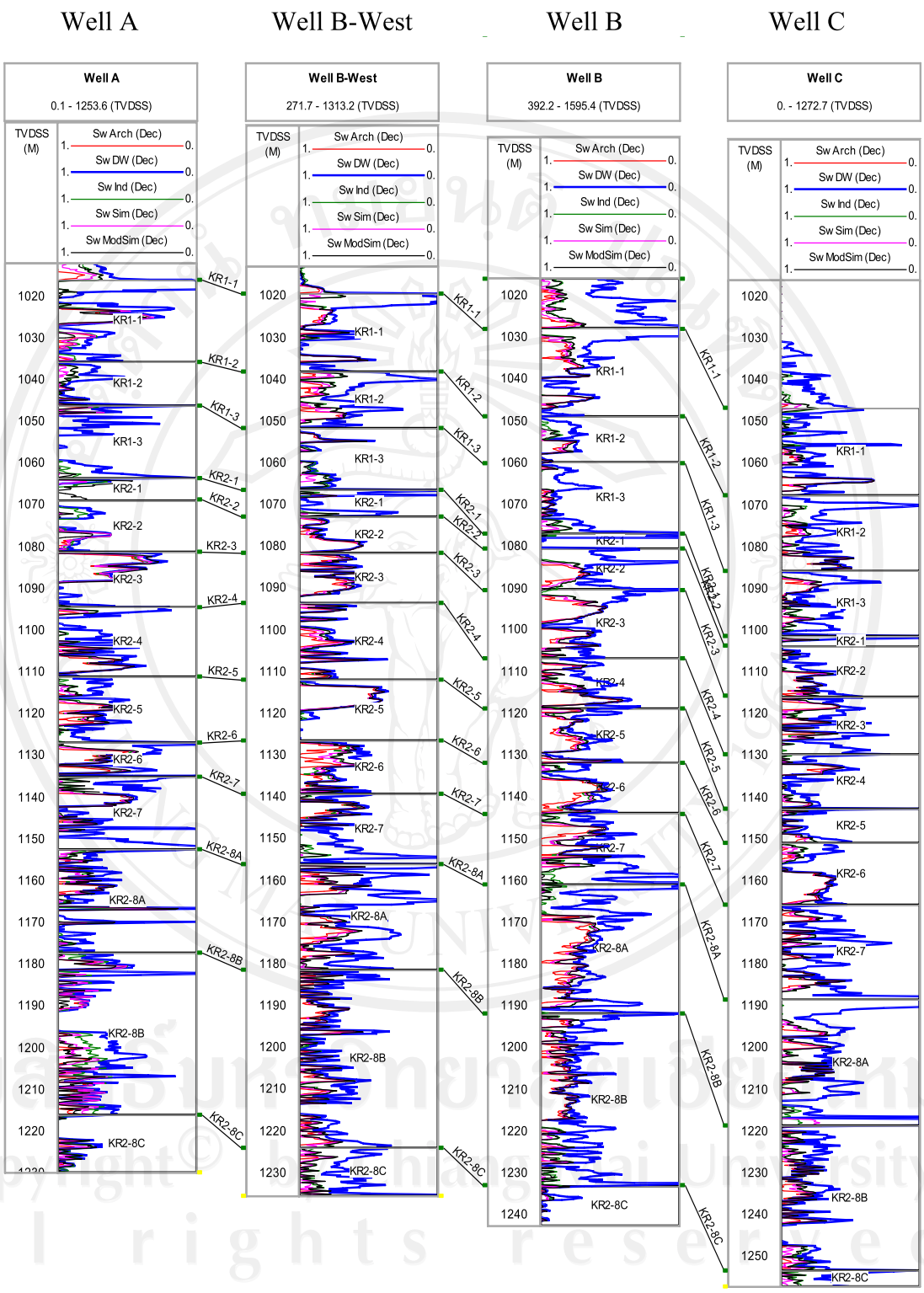

Figure 3.21 Comparison of the estimated water saturations by various shaly sand models (reservoir units are flattened on sea level and depth-set with TVDss).

Table 3.6 Comparison of shaly sand "Sw" models (unit in percentage), arithmetic average gross Sw values of reservoir units, DW = Dual water model, Arc. = Archie model, Sim. = Simandaux model, M.Sim. = Modified Simandaux model, Indo. = Indonesian model.

Well	Res. Units/ Sw Models	KR 1-1	KR 1-2	KR 1-3	KR 2-1	KR 2-2	KR 2-3	KR 2-4	KR 2-5	KR 2-6	KR 2-7	KR 2-8A	KR 2-8B
Well A	DW	72	83	82	93	87	74	66	70	38	57	82	68
	Arc.	92	99	99	100	97	88	94	95	81	93	99	93
	Sim.	90	97	99	97	96	86	91	92	74	91	95	87
	M.Sim	93	93	98	79	99	83	89	89	70	86	92	91
	Indo.	88	93	97	92	92	86	88	89	73	89	93	80
Well B-West	DW	76	56	88	78	81	71	80	72	66	69	52	75
	Arc.	93	92	98	100	89	81	92	76	89	93	88	94
	Sim.	91	87	96	100	86	77	88	76	77	91	82	90
	M.Sim.	89	81	91	96	83	75	84	75	74	89	80	88
	Indo.	89	81	89	95	83	75	84	75	76	89	81	88
Well B	DW	71	83	81	91	57	61	59	72	76	54	61	69
	Arc	89	95	99	100	91	82	86	84	93	92	85	93
	Sim.	87	93	97	100	87	79	82	81	87	87	81	90
	M.Sim.	85	91	94	100	85	77	80	79	85	81	79	88
	Indo.	85	90	93	99	84	77	80	80	86	81	80	87
Well C	DW	80	69	66	85	76	61	81	78	69	67	68	83
	Arc.	98	98	67	98	61	97	98	93	97	99	98	99
	Sim.	97	96	95	97	88	95	97	91	94	98	97	95
	M.Sim.	95	92	92	94	86	91	96	88	89	96	95	91
	Indo.	95	92	91	94	86	91	95	88	87	96	93	90

3.8 Reservoir Summation

The reservoir summation was established on the determination of cut-off criteria. The effective criteria to classify reservoir and non-reservoir are volume of shale (Vsh), effective porosity (ϕ_e), and water saturation (Sw). Reservoir zones were verified on its definite properties within acceptable ranges such as Vsh and ϕ_e. Reservoirs with sufficient capacity to allow fluid at acceptable volume of hydrocarbon are commercially classified as a potential reservoir or net pay zone.

Production analysis, drill-stem test, special logging tools such as nuclear magnetic resonance, and laboratory analysis of core samples are helpful to identify the net pay zones. Only well log derived parameters are available to concern the reservoir characters and to determine hydrocarbon intervals in this study. To identify net reservoirs and net pay hydrocarbon zones, the following categories were relevant for these reservoir units.

- Gross is the gross thickness of reservoir unit by top and bottom intervals.
- Effective reservoir is defined with less than 30% of Vsh values and having greater than 8% of ϕ_e.
- The net-pay hydrocarbon interval, properties of net reservoir and less than 60% of Sw are valid to separate hydrocarbon bearing intervals.
- N/R is the ratio of net pay intervals and effective reservoir thickness.
- ϕ_e (effective porosity, fraction) is greater than 8% of shale corrected ϕ_e of net reservoir units.
- Vsh (volume of shale, fraction) is less than 30% of Vsh for effective reservoir units.
- Sw (dual water saturation, fraction) is less than 60% of Sw for net pay zones.

Table 3.7 to Table 3.10 lists the summation of reservoir units for studied wells.

Table 3.7 Well A, summary of the average gross, net reservoir and net pay.

Units	KR 1-1	KR 1-2	KR 1-3	KR 2-1	KR 2-2	KR 2-3	KR 2-4	KR 2-5	KR 2-6	KR 2-7	KR 2-8A	KR 2-8B
Gross (m)	20	10	18	5	12	13	16	16	8	17	25	39
Eff. Res. (m)	16	10	14	4	7	13	15	15	7	12	20	30
Net Pay (m)	4	0.4	1.3	0	0	5	5	2.4	4	5	1.4	6.3
N/R (fraction)	0.3	0.1	0.1	0	0	0.4	0.3	0.2	0.6	0.4	0.1	0.2
ϕe (%)	22	26	19	16	25	15	13	14	12	13	14	14
Vsh (%)	10	10	15	20	7	8	10	12	7	9	14	13
Sw (%)	40	54	47	-	-	40	48	51	37	46	56	54

Table 3.8 Well B-West, summary of the average gross, net reservoir and net pay.

Units	KR 1-1	KR 1-2	KR 1-3	KR 2-1	KR 2-2	KR 2-3	KR 2-4	KR 2-5	KR 2-6	KR 2-7	KR 2-8A	KR 2-8B
Gross (m)	19	14	15	6	9	12	18	15	13	17	25	43
Eff. Res. (m)	15	11	11	0.6	9	12	14	13	6	3	18	24
Net Pay (m)	2	5	0.3	0	2	4	1	5	4	0.7	11	5
N/R (fraction)	0.1	0.5	0.03	0	0.2	0.3	0.1	0.4	0.7	0.2	0.6	0.2
ϕe (%)	20	19	19	17	22	17	15	15	10	9	13	11
Vsh (%)	10	12	16	18	6	7	14	11	14	13	9	11
Sw (%)	53	48	51	-	56	56	53	44	53	51	40	48

Table 3.9 Well B, summary of the average gross, net reservoir and net pay.

Units	KR 1-1	KR 1-2	KR 1-3	KR 2-1	KR 2-2	KR 2-3	KR 2-4	KR 2-5	KR 2-6	KR 2-7	KR 2-8A	KR 2-8B
Gross (m)	21	13	16	4	10	16	12	13	12	17	31	41
Eff. Res. (m)	19	11	15	2	7	15	12	13	11	12	27	39
Net Pay (m)	3	0	0.3	0	2	6	5	2	5	6	9	6
N/R (fraction)	0.2	0	0.02	0	0.29	0.3	0.4	0.2	0.5	0.5	0.3	0.2
ϕe (%)	24	25	21	16	26	21	17	23	17	15	20	15
Vsh (%)	9	10	12	19	11	7	9	6	10	13	7	8
Sw (%)	48	-	56	-	53	52	49	49	54	47	52	54

Table 3.10 Well C, summary of the average gross, net reservoir and net pay.

Units	KR 1-1	KR 1-2	KR 1-3	KR 2-1	KR 2-2	KR 2-3	KR 2-4	KR 2-5	KR 2-6	KR 2-7	KR 2-8A	KR 2-8B
Gross (m)	21	18	16	3	12	14	13	8	15	23	28	36
Eff. Res. (m)	18	17	15	2	12	12	13	8	15	21	22	34
Net Pay (m)	2	4	4	0.14	1.4	6.4	1.3	0.7	1.6	6.1	6.4	1.0
N/R (fraction)	0.1	0.2	0.3	0.1	0.1	0.5	0.1	0.1	0.1	0.3	0.3	0.03
ϕe (%)	21	19	24	17	22	19	17	16	19	14	13	15
Vsh (%)	8	9	9	16	7	12	6	7	7	8	11	10
Sw (%)	45	53	51	56	49	51	53	54	58	48	54	56

Figures 3.22 to Figure3.25 summarize composite well logs for the studied wells.

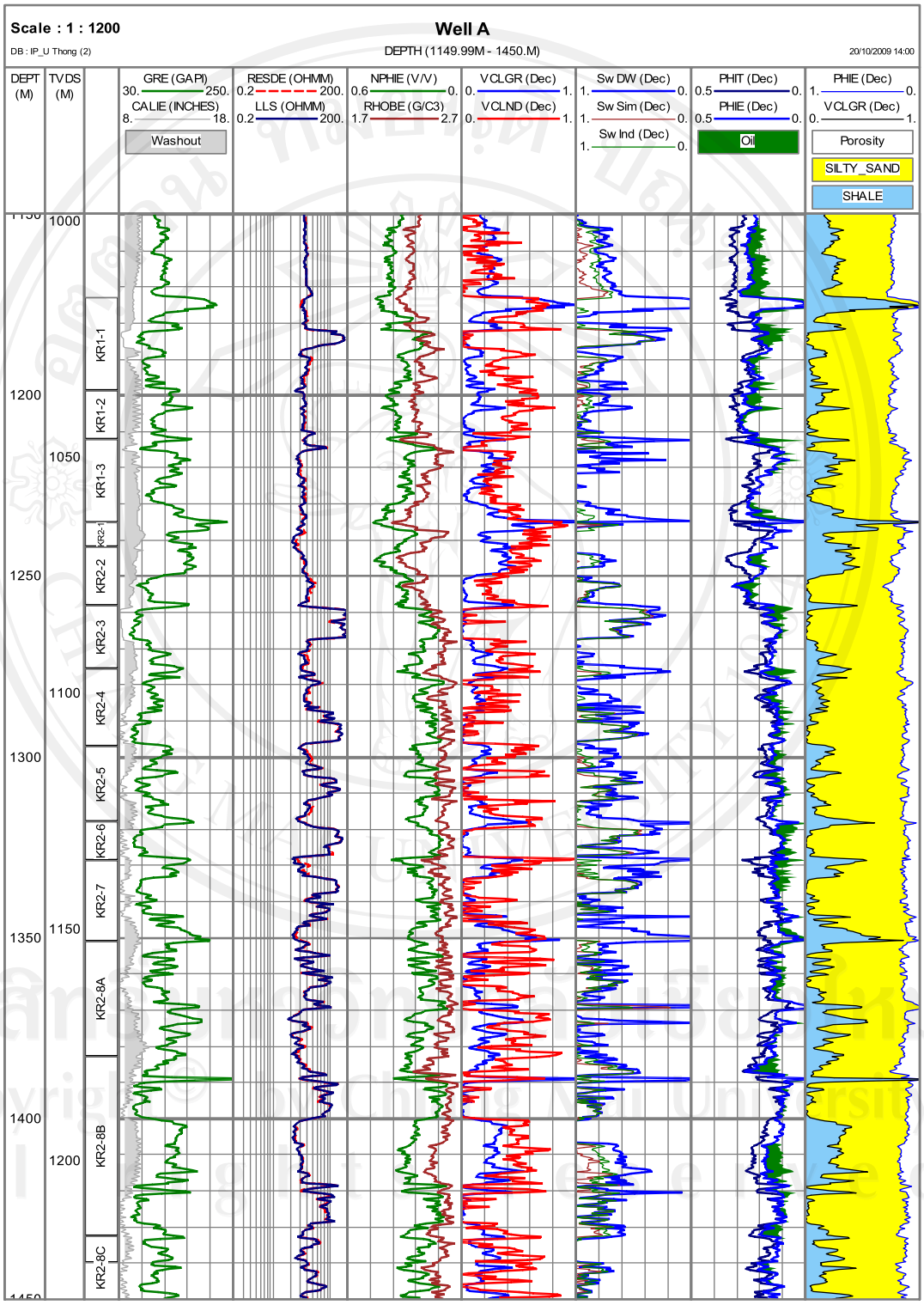

Figure 3.22 Well A, composite log with petrophysical interpretation.

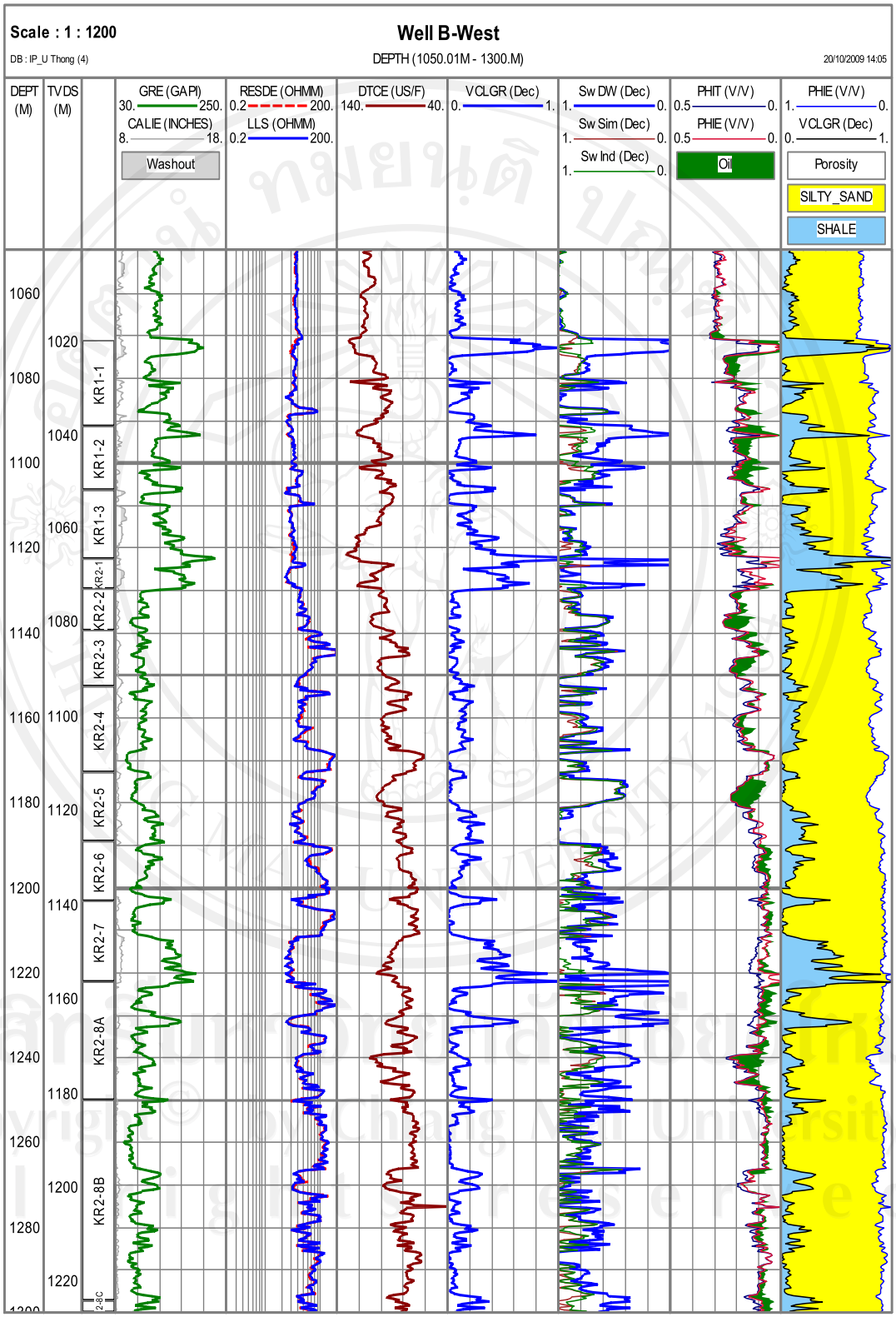

Figure 3.23 Well B-West, composite log with petrophysical interpretation.

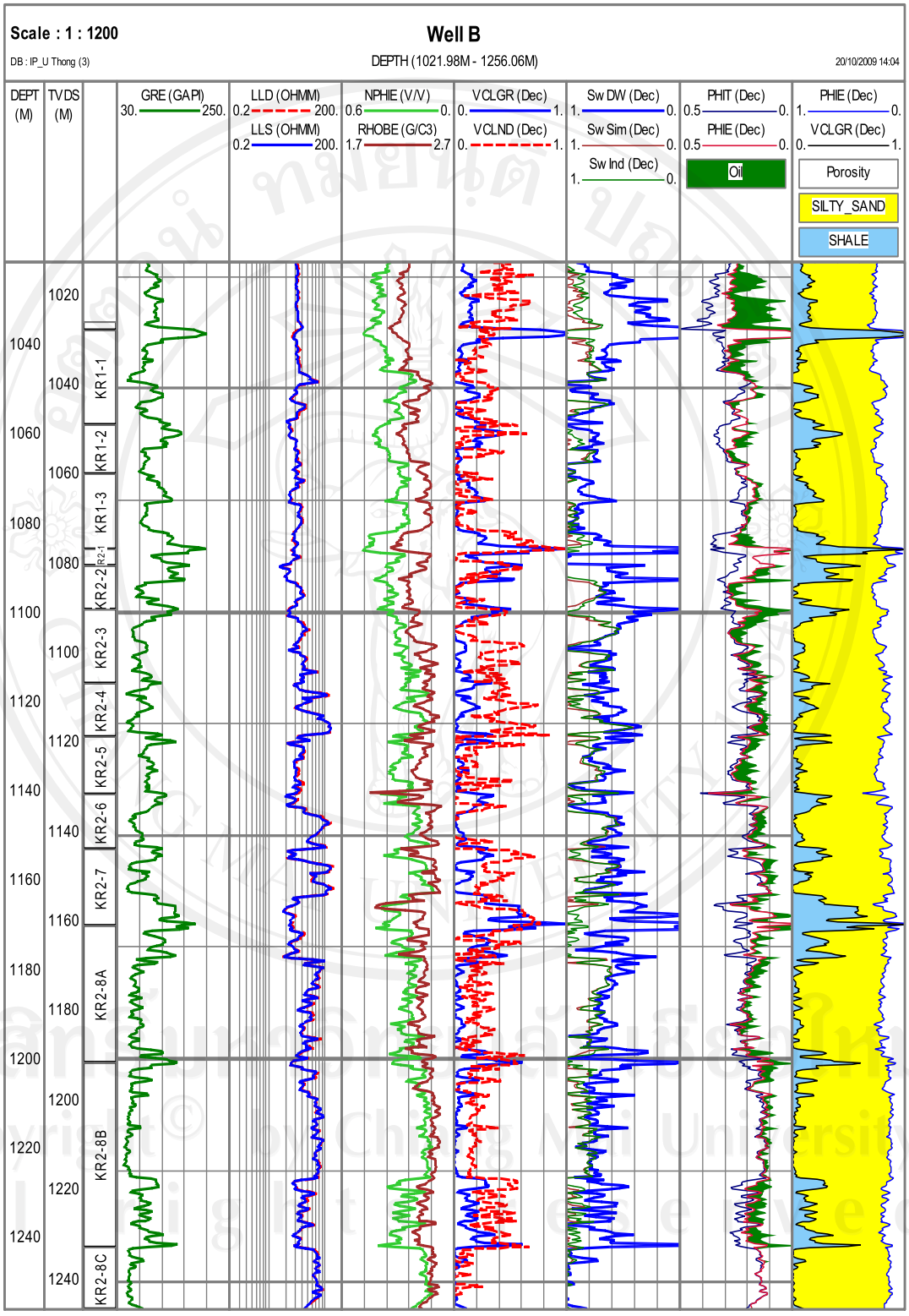

Figure 3.24 Well B, composite log with petrophysical interpretation.

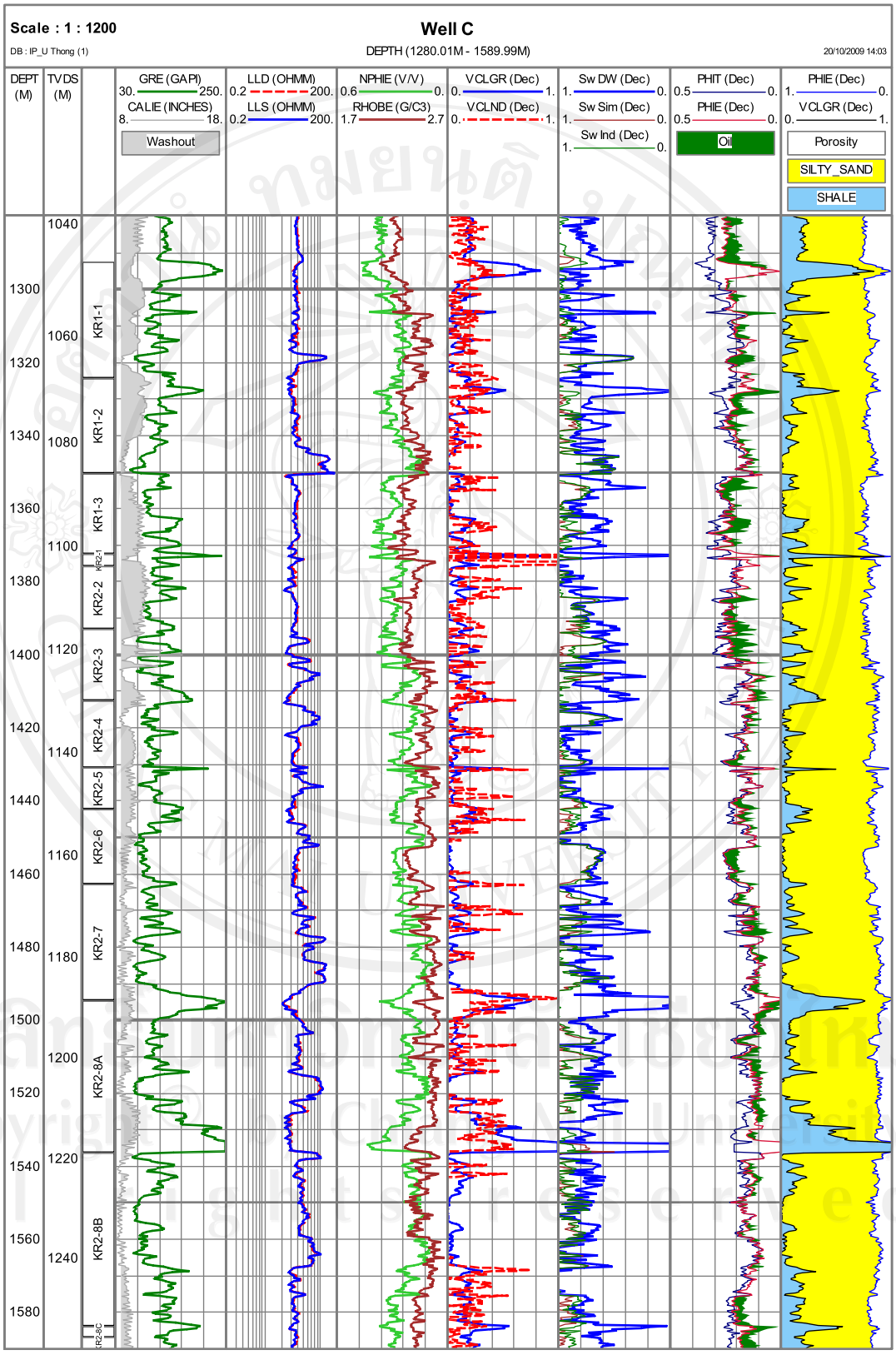

Figure 3.25 Well C, composite log with petrophysical interpretation.

3.9 Electrofacies

The electrofacies analysis is fundamentally based on gamma ray, sonic, resistivity, neutron, and density logs. Gamma ray log shapes are especially used to interpret sedimentary cycles and depositional facies. The five log patterns of gamma ray are referenced to Rider (1996). These patterns are bell shape (sharp base and fining upward), funnel shape (coarsening upward and sharp top), blocky or cylindrical shape (consistently low gamma values with sharp base and top), bow shape (symmetric increasing and decreasing of gamma ray readings) and irregular or serrated pattern (no systematic changes). The gamma ray log detects the natural radioactivity of rocks and corresponds to grain size. Therefore, the gamma ray log makes possible qualitative verification between fine grained and coarse grained textures. Lithologic break and/or unconformities and formation boundaries could be traced by the abrupt changes of gamma ray patterns.

The studied wells were divided into three division of facies group of potential reservoirs. These division boundaries were identified based on shale baseline value of gamma ray, peak and spike gamma ray reading supported by sonic pattern.

- The upper facies division is dominated by coarsening upward shape.
- The middle part of facies group irregular blocky, fining upward and coarsening upward shape.
- The lower part of facies group irregular blocky pattern facies.

The gross thickness of facies units are defined based on the true vertical depth (mTVD).

Figure 3.26 to Figure 3.29 show the interpretation of facies and expected depositional environments for studied wells.

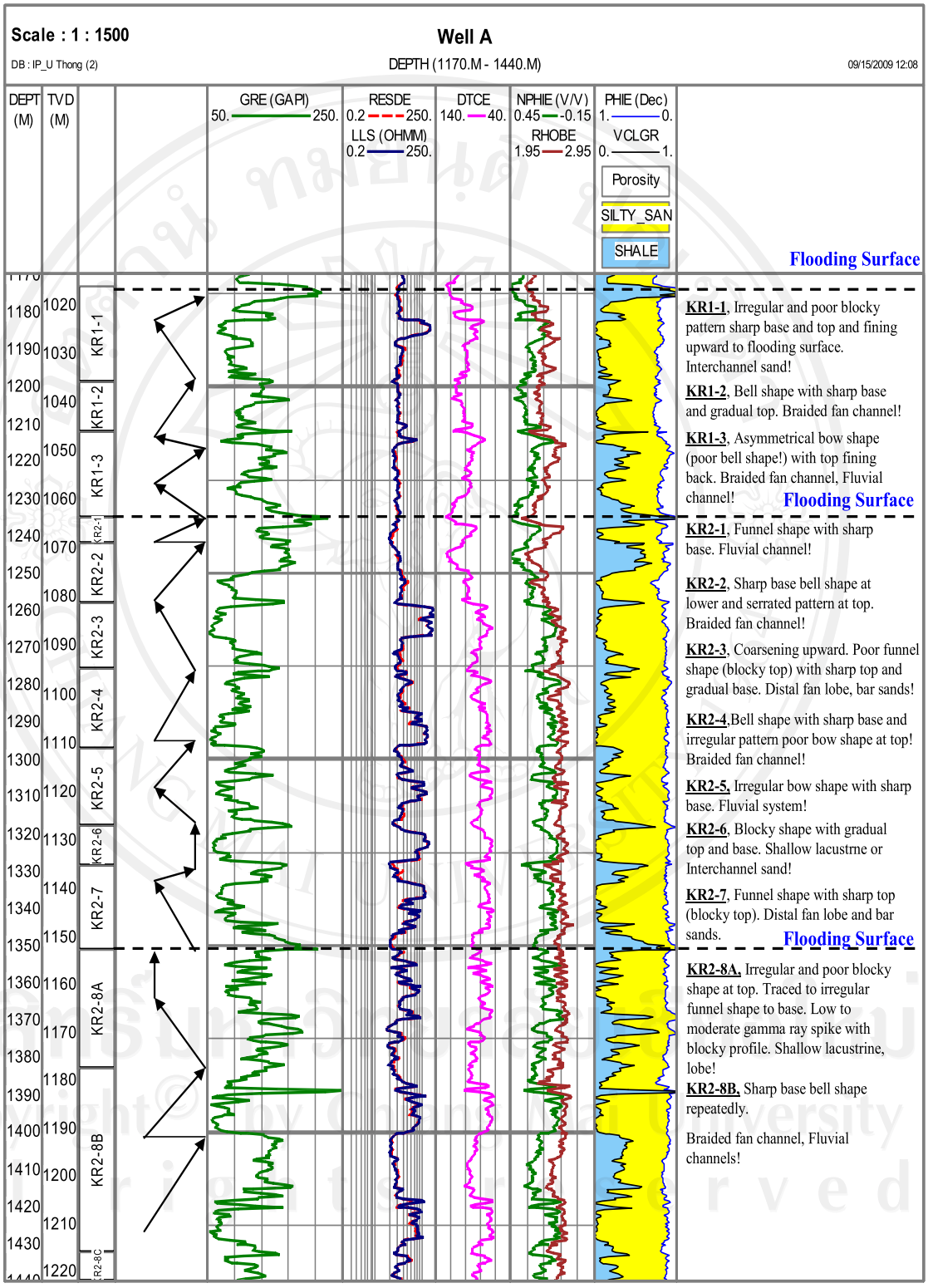

Figure 3.26 Interpretation of facies and expected depositional environments, well A.

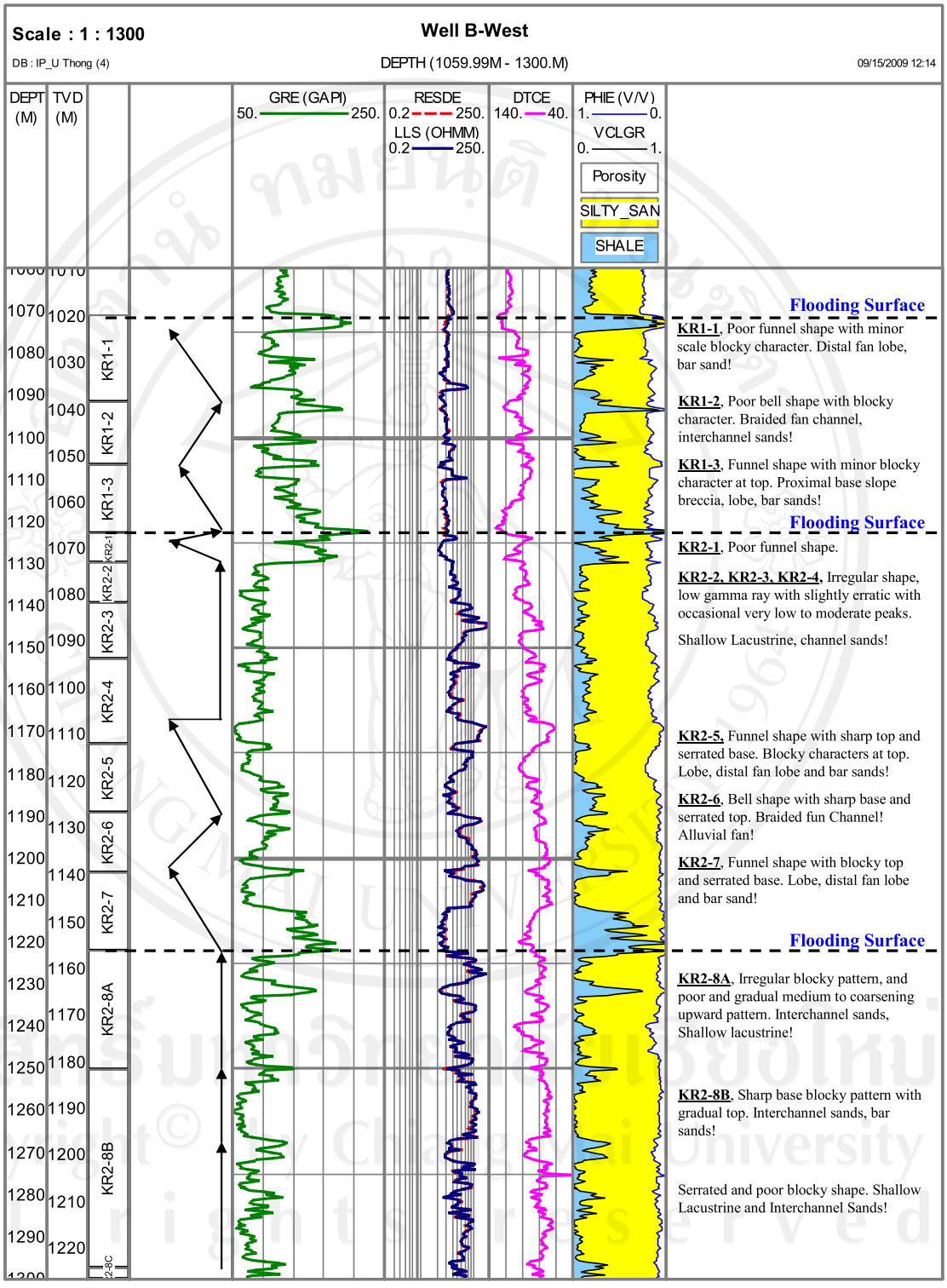

Figure 3.27 Interpretation of facies and expected depositional environments, well B-West.

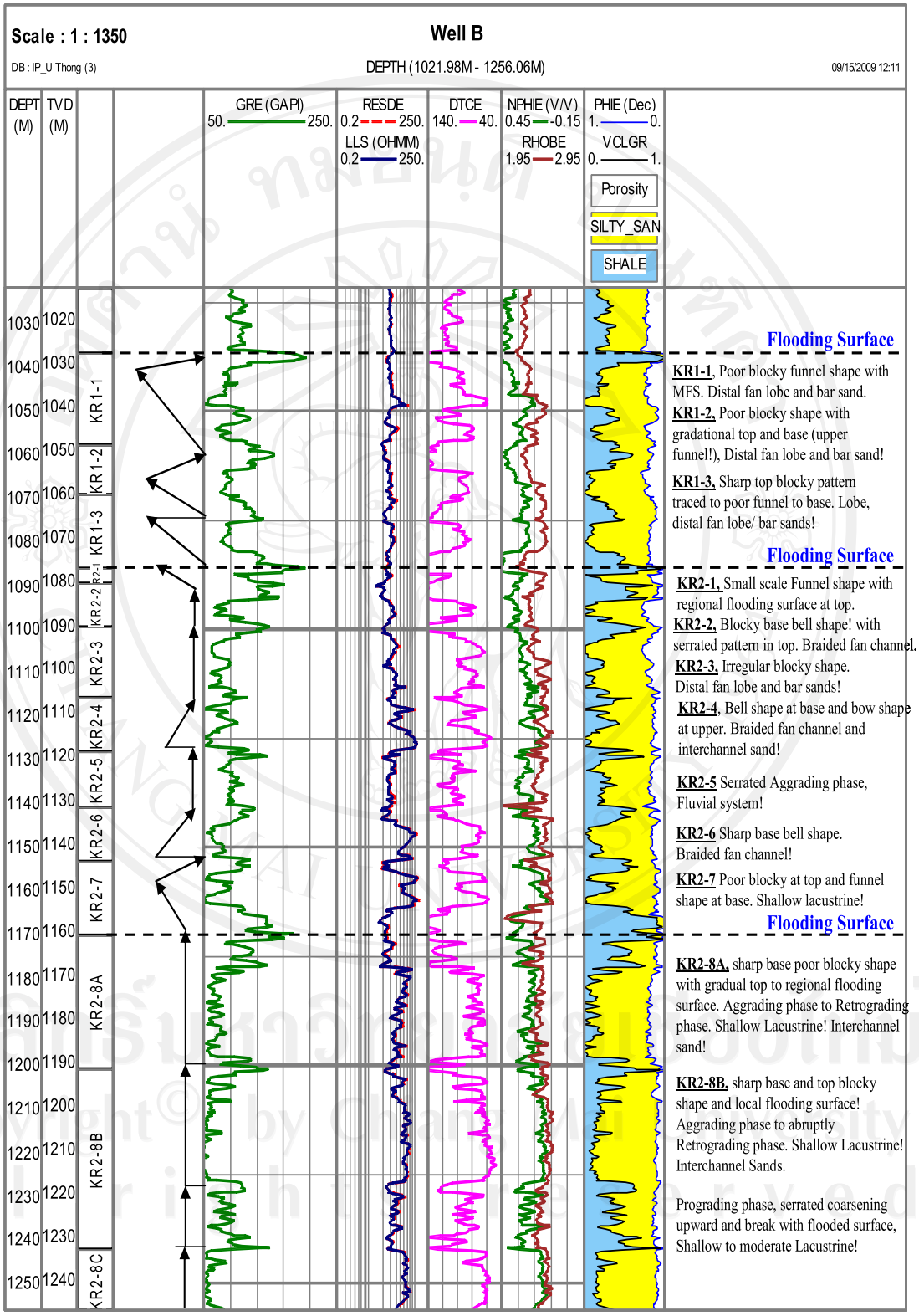

Figure 3.28 Interpretation of facies and expected depositional environments, well B.

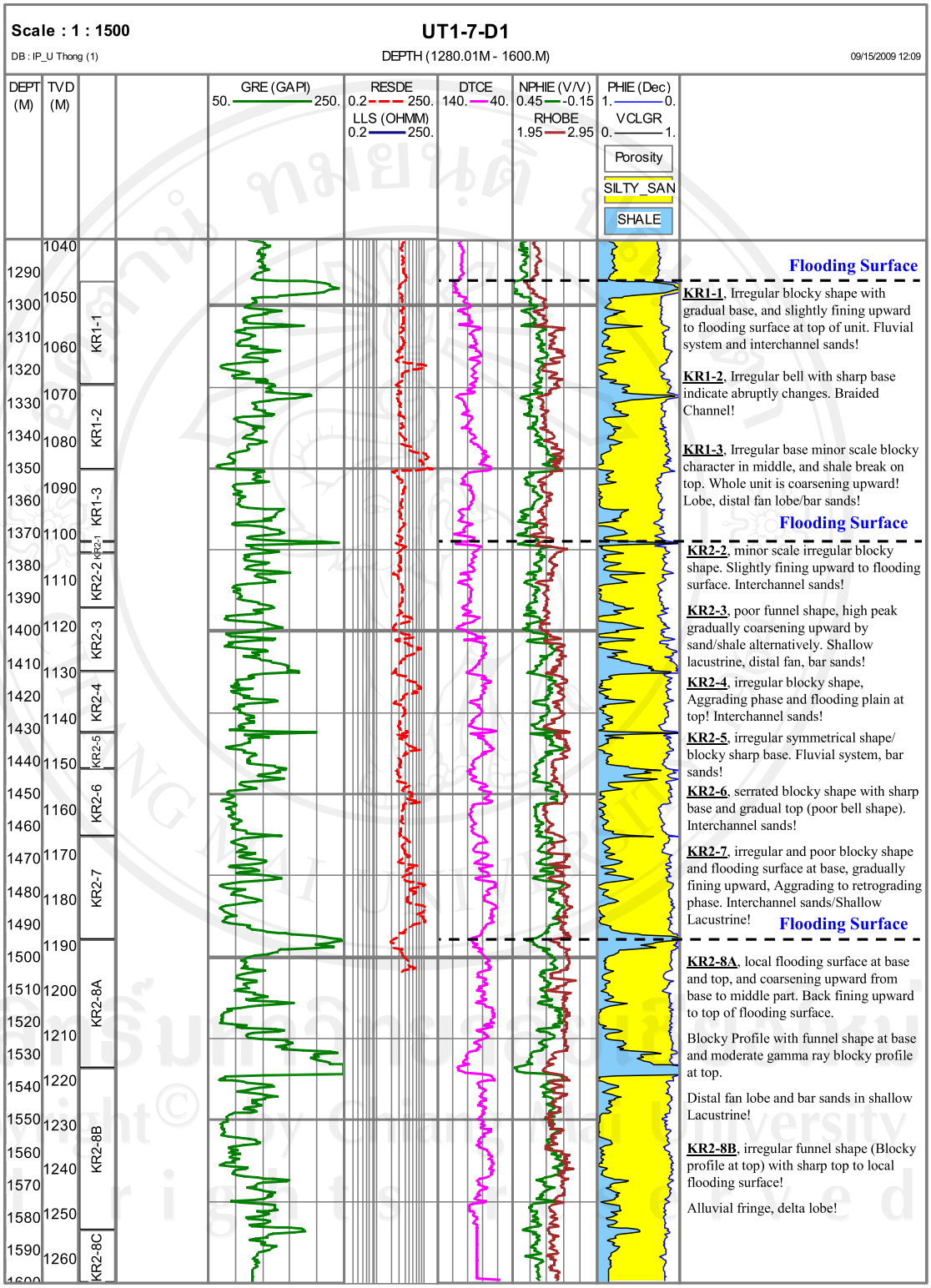
Scale : 1 : 1500
UT1-7-D1
DB : IP_U Thong (1)
DEPTH (1280.01M - 1600.M)
09/15/2009 12:09
DEPT (M)
TVD (M)
GRE (GAPI)
50. 250.
RESDE
0.2 250.
LLS (OHMM)
0.2 250.
DTCE
140. 40.
NPHIE (V/V)
0.45 -0.15
RHOBE
1.95 2.95
PHIE (Dec)
1. 0.
VCLGR
0. 1.
Porosity
SILTY_SAN
SHALE
KR1-1
KR1-2
KR1-3
KR2-1
KR2-2
KR2-3
KR2-4
KR2-5
KR2-6
KR2-7
KR2-8A
KR2-8B
KR2-8C
Flooding Surface
KR1-1, Irregular blocky shape with gradual base, and slightly fining upward to flooding surface at top of unit. Fluvial system and interchannel sands!
KR1-2, Irregular bell with sharp base indicate abruptly changes. Braided Channel!
KR1-3, Irregular base minor scale blocky character in middle, and shale break on top. Whole unit is coarsening upward! Lobe, distal fan lobe/bar sands!
Flooding Surface
KR2-2, minor scale irregular blocky shape. Slightly fining upward to flooding surface. Interchannel sands!
KR2-3, poor funnel shape, high peak gradually coarsening upward by sand/shale alternatively. Shallow lacustrine, distal fan, bar sands!
KR2-4, irregular blocky shape, Aggrading phase and flooding plain at top! Interchannel sands!
KR2-5, irregular symmetrical shape/ blocky sharp base. Fluvial system, bar sands!
KR2-6, serrated blocky shape with sharp base and gradual top (poor bell shape). Interchannel sands!
KR2-7, irregular and poor blocky shape and flooding surface at base, gradually fining upward, Aggrading to retrograding phase. Interchannel sands/Shallow Lacustrine!
Flooding Surface
KR2-8A, local flooding surface at base and top, and coarsening upward from base to middle part. Back fining upward to top of flooding surface.
Blocky Profile with funnel shape at base and moderate gamma ray blocky profile at top.
Distal fan lobe and bar sands in shallow Lacustrine!
KR2-8B, irregular funnel shape (Blocky profile at top) with sharp top to local flooding surface!
Alluvial fringe, delta lobe!